conducted in triplicate. The quantity of each transcript was calculated according to the instrument's manual and normalized to the amount of GAPDH mRNA. Amplification without template was included as a control.

Results

Tax1 interacts with MAGI-1 through the PBM. To determine any unidentified Tax1 PBM interacting proteins, a GST fusion protein of Tax1 versus that of its PBM-deletion mutant (Tax1ΔC) were used (Fig. 1A). Proteins bound to Tax1 but not to Tax1ΔC were analyzed by mass spectrometry, and MAGI-1 was identified as one of the Tax1 PBM interacting partners. In order to confirm the interaction of Tax1 with MAGI-1, Tax1 or Tax1ΔC expression plasmids were transiently transfected into the 293T cells or they were co-transfected with the FLAG-tagged MAGI-1 expression plasmid by the lipofection method (FUGENE 6). At 48 h after transfection, cell lysates were immunoprecipitated with anti-Tax1 antibody. The amount of MAGI-1 or FLAG in immunoprecipitates was analyzed by a Western blotting analysis (Fig. 1B,C). MAGI-1 was co-immunoprecipitated only with Tax1 but not with Tax1ΔC (Fig. 1B, IP: Tax1). As will be shown later, the amount of detergent-soluble MAGI-1 protein is reduced by wild type Tax1 but not Tax1ΔC (Fig. 1B). In addition to endogenous MAGI-1, exogenously transduced MAGI-1 was also efficiently co-immunoprecipitated with Tax1 but not with Tax1ΔC (Fig. 1C, IP: Tax1). These results indicate that Tax1 can interact with MAGI-1, and this interaction is dependent on the presence of the PBM in Tax1.

Tax1 alters the subcellular localization of MAGI-1. To further establish the association of Tax1 with MAGI-1 *in vivo*, the subcellular localization of both proteins was examined. The 293T cells were grown on cover slips overnight, followed by transient transfection with Tax1 plasmids. At 48 h after the transfection, the cells were stained with anti-Tax1 and anti-MAGI-1, and their subcellular localization was analyzed by fluorescent microscopy. On its own, MAGI-1 was primarily located in the cytoplasm and on the membrane (Fig. 2, Control). In the presence of Tax1, MAGI-1 colocalized with Tax1 as particular spots (yellow in color), mainly in the perinuclear region of the cytoplasm (Fig. 2, Tax1). In contrast, Tax1 PBM deletion mutant did not obviously show colocalization with MAGI-1 and did not alter the subcellular localization (Fig. 2, Tax1ΔC). We and others have shown a similar behavior of Tax1 with other PDZ proteins such as MAGI-3, Dlg1 and Scribble.[14,45,46] Taken together, our results indicate that Tax1 mislocalizes MAGI-1 by aberrantly sequestering it within Tax1 containing complexes.

Tax1 translocates MAGI-1 from the detergent-soluble to the detergent-insoluble cellular fraction. Several oncoproteins of tumor viruses inactivate functions of cellular tumor suppressor proteins by altering their subcellular localizations.[13,30,37,46,47] We therefore went ahead to investigate the subcellular localization of MAGI-1 in the presence of Tax1 by cell fractionation assay. At first, 293T cells transiently transfected with Tax1 or Tax1ΔC were lysed by a mild detergent (NP40). The NP40-insoluble fraction was further lysed by the SDS-sample buffer, and then the NP40-soluble fraction, the NP40-insoluble fraction and the total fraction directly lysed by the SDS-sample buffer were separately collected. The amounts of endogenous MAGI-1 and transduced Tax1 protein in these three fractions were measured by a Western blotting analysis. MAGI-1 in 293T cells transfected with Tax1ΔC was dominantly detected in the soluble fraction, with a smaller amount in the insoluble fraction, and the amounts were almost equivalent to those in cells transfected with the control plasmid (Fig. 3A, lane 1, 3). On the other hand, while MAGI-1 in the soluble fraction of cells was drastically reduced by transfection of Tax1, MAGI-1 in the insoluble fraction was greatly increased (Fig. 3A, lane 2). Total MAGI-1 protein was unaffected by expression of Tax1 or Tax1ΔC (Fig. 3A, top panel). Similarly, when we examined HTLV-1-infected human T-cells (SLB-1) and uninfected human T-cells (Jurkat), MAGI-1 was detected in the insoluble fraction of SLB-1 with high expression of Tax1 but not that in Jurkat (Fig. 3B). Taken together, our results show that Tax1 induces the translocation of MAGI-1 from the detergent-soluble to the detergent-insoluble cellular fraction. Note worthy MAGI-1 in the insoluble fraction of SLB-1 was detected as a higher molecular weight band than MAGI-1 in the soluble one. This is likely to be due to the post-transcriptional modification of MAGI-1 similar to the phosphorylation reported for Dlg1 in HTLV-1-infected T-cells.[13,14]

Downregulation of MAGI-1 protein during Tax1-induced transformation. We next investigated whether Tax1-induced transformation alters MAGI-1 expression. CTLL-2 is a mouse T-cell line, and it is widely used in HTLV-1 research due to its transformation by Tax1 from IL-2-dependent into IL-2-independent growth.[6,15] Transient expression of Tax1 or Tax1ΔC in CTLL-2 and Jurkat cells barely affected MAGI-1 expression (Fig. 4A). In addition, stable expression of Tax1 in CTLL-2 cells in the presence of IL-2 little affected the expression of MAGI-1 (Fig. 4B, left panel). On the other hand, MAGI-1 expression in Tax1-transformed IL-2-independent

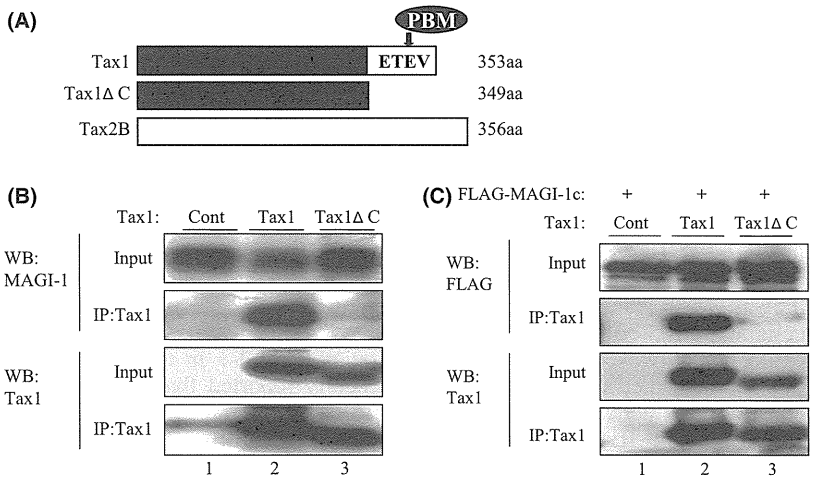

Fig. 1. Tax1 interacts with MAGI-1 in a PBM-dependent manner. (A) Structures of Tax1, Tax1ΔC and Tax2 proteins used in this study. The amino acid sequence of the PBM is shown. (B, C) 293T cells were transiently transfected with pHβPr-neo-Tax1 (lane 2), pHβPr-neo-Tax1ΔC (lane 3) or pHβPr-neo plasmid (lane 1) together with (C) or without pcDNA3.1:FLAG-MAGI-1c (B) by the lipofection method (FUGENE 6). At 48 h post-transfection, the cells were treated with lysis buffer, and cell lysates immunoprecipitated with anti-Tax1 antibody. Total cell lysates (Input) and immunoprecipitates (IP: Tax1) were characterized by a Western blotting analysis using the indicated antibodies.

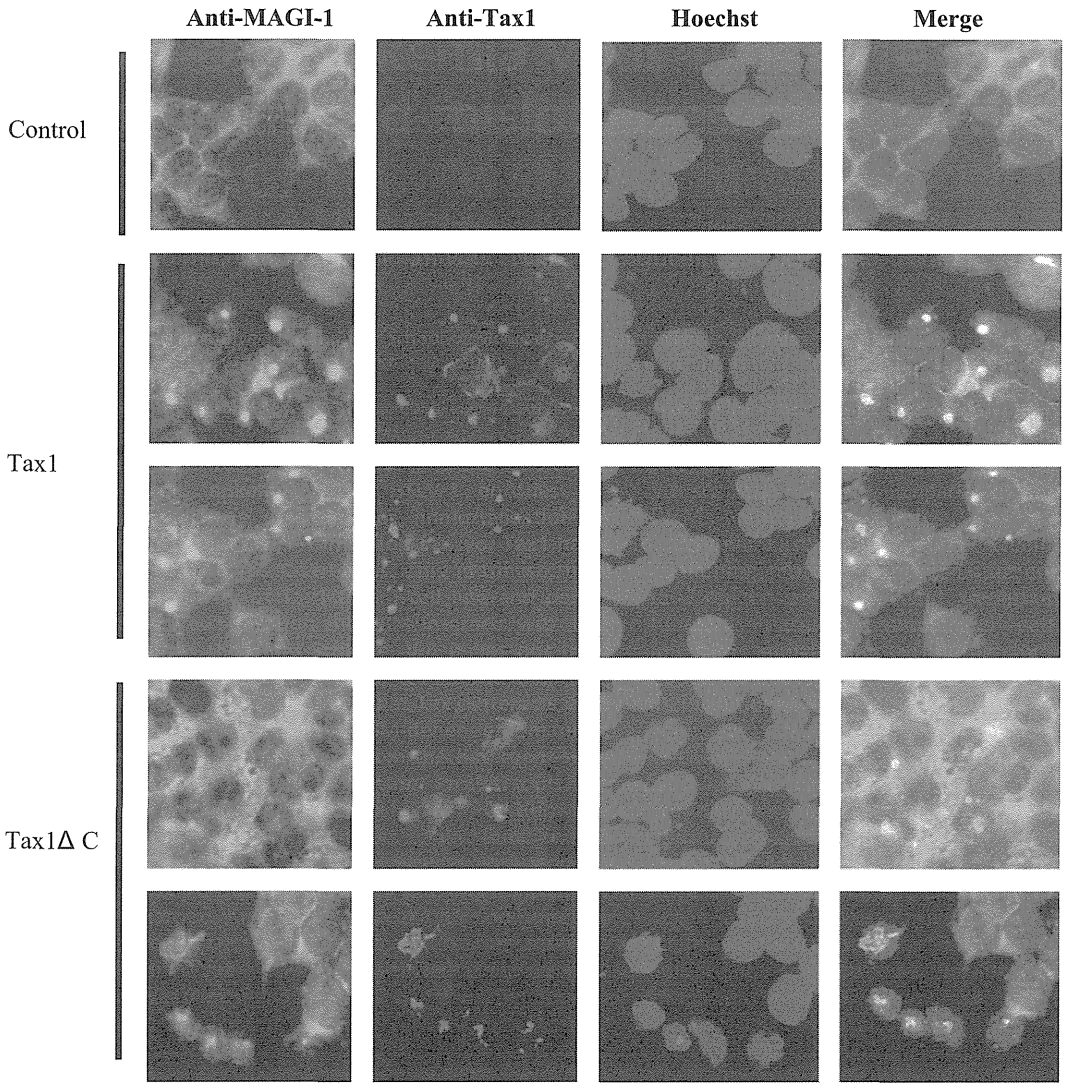

Fig. 2. Subcellular localization of Tax1 and endogenous MAGI-1 in 293T cells. 293T cells were transfected with either the Tax1 or Tax1ΔC plasmid as described in the methods. The cells were stained with anti-Tax1 (red), anti-MAGI-1 (green), and Hoechst 33258 (blue) for nuclear staining. The stained cells were examined by fluorescent light microscopy.

CTLL-2 cells was much lower than that of their untransformed counterparts (Fig. 4B, right panel, Fig. 4C). The expression of another PDZ domain containing protein, syntrophin, with which Tax1 also interacts (Higuchi M, unpublished data, 2006), was intact in Tax1-transformed CTLL-2 cells (Fig. 4C), indicating that MAGI-1 reduction in Tax1-transformed cells was a specific phenomenon. A real-time RT-PCR assay showed that MAGI-1 downregulation occurred at the transcriptional level, as shown by the almost undetectable corresponding mRNA levels (Fig. 4D). We previously reported that Tax1ΔC also transforms CTLL-2, but the activity was much lower than that of Tax1.[15] Contrary to our expectations, Tax1ΔC also induced downregulation of MAGI-1 (Fig. 4C lanes 7–9). To examine if MAGI-1 downregulation in Tax1-transformed CTLL-2 cells is a consequence of IL-2 withdrawal, we restored IL-2 in the cultures of Tax1-transformed cells and checked for the MAGI-1 expression. IL-2 restoration could not, however, rescue the expression of MAGI-1 in two Tax1-transformed cells (Fig. 5A). We recently reported that a constitutively active Akt1 oncoprotein (hAkt1ΔPH) transforms CTLL-2 from IL-2-dependent growth into IL-2-independent growth.[39] Like Tax1, MAGI-1 expression in Akt1-transformed IL-2-independent cells was also downregulated as compared to the untransformed CTLL-2 cells growing in the presence of IL-2, and restoration of IL-2 failed to rescue MAGI-1 expression in these transformed cells like Tax1-transformed cells (Fig. 5B). These results suggest that Tax1-transformation of CTLL-2 cells is associated with an irreversibly downregulated expression of MAGI-1.

Human T-cell leukemia virus type 1 has been shown to immortalize and transform human T-cells in an IL-2-dependent and IL-2-independent manners, respectively.[9,10,16] These findings prompted us to examine the expression status of MAGI-1 in human T-cells. As shown, all five HTLV-1-transformed T-cell lines including one transformed by HTLV-1 with a Tax1 PBM deletion mutant showed lower amounts of MAGI-1 compared to the three HTLV-1-negative cell lines (Fig. 6A). Similar to the observation in Tax1-transformed CTLL-2 cells, a real-time RT-PCR analysis showed that MAGI-1 mRNA was significantly reduced in HTLV-1-infected cells as compared to the HTLV-1-uninfected ones (Fig. 6B). HTLV-2 is a close ally of HTLV-1, exhibiting more than 70% similarity at the nucleotide sequence level. Intriguingly, HTLV-2 does not cause any leukemia or lymphoma in spite of its ability to immortalize

doi: 10.1111/cas.12087

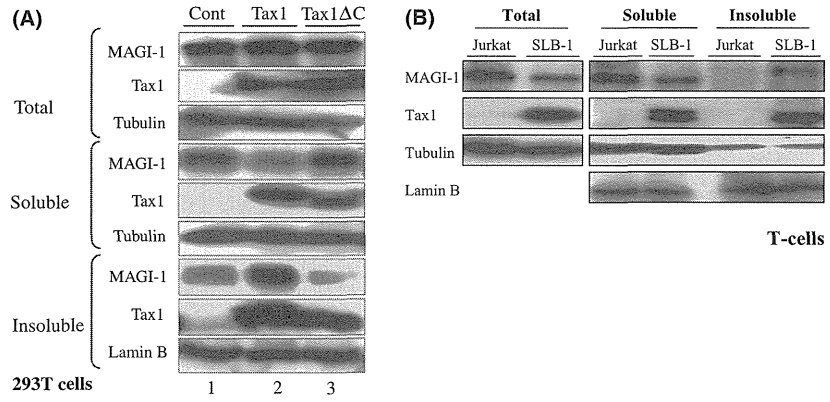

Fig. 3. Tax1 translocates MAGI-1 from the soluble to the insoluble cellular fraction. (A) The 293T cells transfected with Tax1 (lane 2), Tax1ΔC (lane 3) or control (lane 1) were divided into two groups. One group was treated with the NP40 lysis buffer and fractionated as described in Materials and Methods. The other group was directly treated with the sodium dodecyl sulfate (SDS)-sample buffer and used as the total fraction. The three types of samples were size-fractionated by SDS-polyacrylamide gel electrophoresis (PAGE) followed by a Western blotting analysis. (B) Cell lysates from the total, soluble and insoluble fractions of Jurkat and SLB-1 cells were prepared as describe in (A) and the amounts of MAGI-1, Tax1, Tubulin and Lamin B proteins in the lysates were measured by a Western blotting analysis.

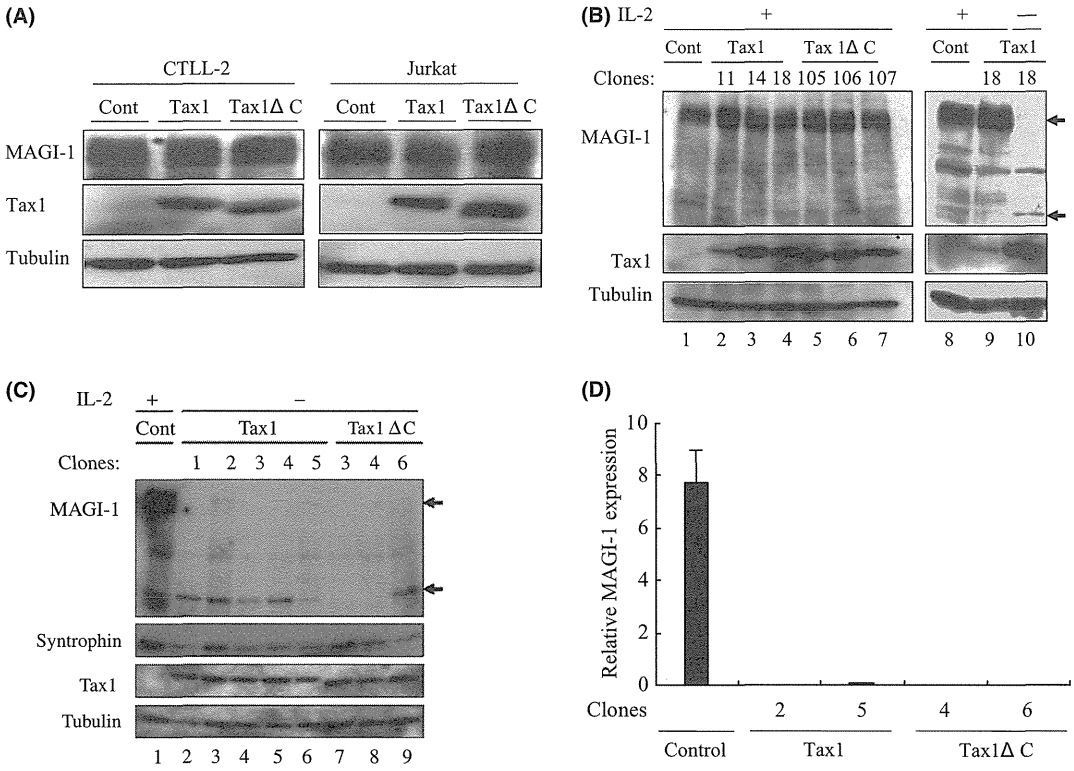

Fig. 4. MAGI-1 downregulation by interleukin (IL)-2-independent transformation of T-cells. (A) CTLL-2 and Jurkat cells were transfected with lentiviruses encoding Tax1. At 48 h after transfection, cell lysates were prepared and the amounts of MAGI-1, Tax1 and Tubulin were determined by a Western blotting analysis. (B) CTLL-2 cells stably expressing Tax1 established as previously described[15] were used as IL-2-dependent cells (lane 2–9). All the above cells were then transferred to IL-2 deficient medium and cultured for more than 1 month. Only one Tax1 expressing clone (Tax1–18) survived in the absence of IL-2 (right panel, lane 10). Cell lysates were prepared from the indicated cells, and protein expression was measured by a Western blotting analysis. (C) CTLL-2 cells transformed by Tax1 and Tax1ΔC were established as described previously.[34] Cell lysates were prepared from these Tax1-transformed (lanes 2–6), Tax1ΔC-transformed (lanes 7–9) and parental CTLL-2 cells (lane 1), and the expressions of MAGI-1, Tax1, Syntrophin-β and Tubulin proteins were measured by a Western blotting analysis. (D) A set of clones each transformed by either Tax1 or Tax1ΔC was selected from (C) above, and the relative gene expression of MAGI-1 was evaluated by the quantitative real-time polymerase chain reaction (PCR) method. The amounts of MAGI-1 were normalized to those of glyceraldehyde 3-phosphate dehydrogenase (GAPDH) expression. The quantitative results are expressed as mean ± standard deviation (SD) of three values per sample. The experiment was independently carried out twice to confirm reproducibility.

human T-cells in an IL-2-dependent manner *in vitro* as effectively as HTLV-1.[17,48] HTLV-2 Tax2 protein has also been shown to play a crucial role in the immortalization ability of the virus.[17,18,43,49] We established peripheral T-cells immortalized by either Tax1 or Tax2, and the expression of MAGI-1 in these cells was determined. Our data indicated that while

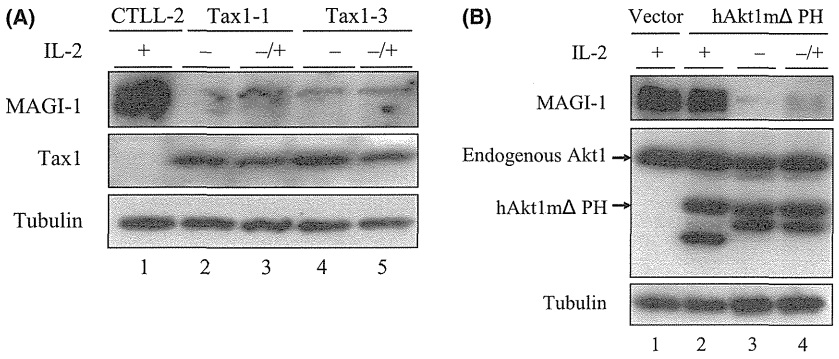

Fig. 5. Restoration of interleukin (IL)-2 cannot rescue MAGI-1 expression in transformed cells. (A) Two distinct Tax1-transformed IL-2-independent CTLL-2 cells (clone 1, 3) were cultured with or without IL-2 for 1 week, and the expression of MAGI-1, Tax1 and Tubulin in the transformed cells with IL-2 (lane 3, 5), the transformed cells without IL-2 (lane 2, 4) and parental CTLL-2 cells with IL-2 (lane 1) were measured by a Western blotting analysis. (B) hAkt1 mΔPH-transformed IL-2-independent CTLL-2 cells were cultured with or without IL-2 for 1 week, and the expressions of MAGI-1, Akt1 and Tubulin proteins in the hAkt1 mΔPH-expressing cells with IL-2 (lane 2), the hAkt1 mΔPH-transformed cells without IL-2 (lane 3), the hAkt1 mΔPH-transformed cells with IL-2 (lane 4) as well as the vector-transduced CTLL-2 cells cultured in the presence of IL-2 (lane 1) were measured by a Western blotting analysis.

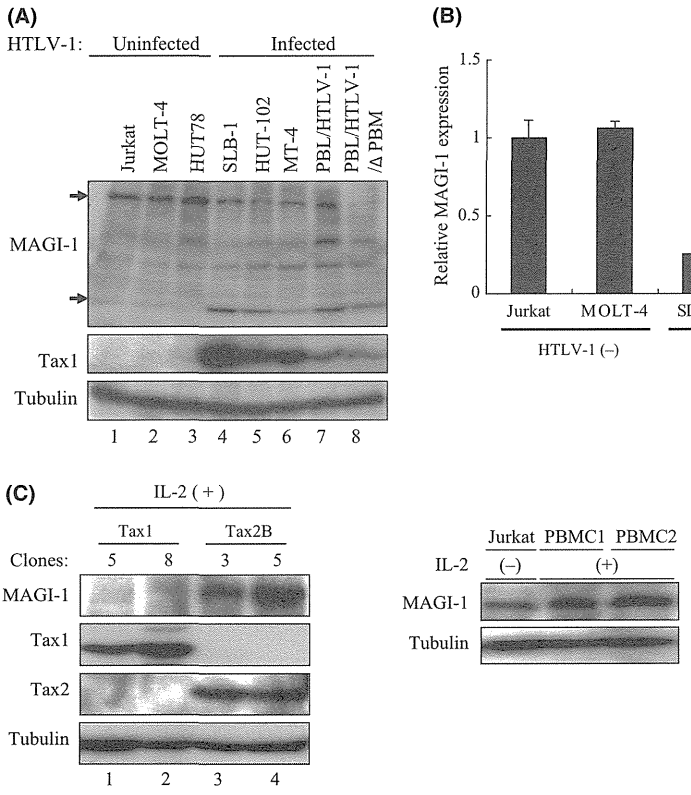

Fig. 6. Expression of MAGI-1 in human T-cell lines transformed by HTLV-1. (A) Cell lysates were prepared from five HTLV-1-transformed (lanes 4–8) and three human T-cell leukemia virus type 1 (HTLV-1)-negative (lanes 1–3) T-cell lines. The lysates were subjected to Western blotting analysis with the antibodies indicated. (B) Expression of MAGI-1 mRNA in two HTLV-1-negative and two HTLV-1-positive cell lines was measured by the quantitative real-time reverse transcription-polymerase chain reaction (RT-PCR) method. The amounts of MAGI-1 were normalized to those of glyceraldehyde 3-phosphate dehydrogenase (GAPDH) expression. The quantitative results are expressed as mean ± standard deviation (SD) of three values per sample. (C) Cell lysates were prepared from two Tax1 and two Tax2-immortalized T-cells (left panel) and HTLV-1 uninfected Jurkat cells and Tax untreated peripheral blood mononuclear cells (PBMCs) (right panel). Western blotting analysis was performed using the corresponding antibodies.

immortalization of human T-cells by Tax1 abolished their expression of MAGI-1, expression of MAGI-1 was intact in those immortalized by Tax2 similar to HTLV-1-uninfected Jurkat and Tax untreated PBMCs (Fig. 6C). Taken together, these findings suggest that the low level MAGI-1 expression phenotype in HTLV-1-transformed cells is as a consequence of Tax1-mediated immortalization of human T-cells. We observed a lower molecular weight product that was recognized by the anti-MAGI-1 antibody in all Tax1- and HTLV-1-transformed T-cells (Figs 4,6), although the identity and the function remains to be clarified.

Discussion

Recent research has focused on the PBM of HTLV-1 Tax1 as a possible determinant of HTLV-1 pathogenesity in reference to the non-leukemogenic HTLV-2 Tax2, which lacks this motif. Tax1 through the PBM has been shown to interact with cellular PDZ domain containing proteins, some of which are implicated in tumor suppression,[31–33] for instance deficiency of Scribble in mice induced prostate cancer through activating MAP kinase pathway.[49] Nevertheless, it remains unclear whether these PDZ proteins explain any of the Tax1 PBM

doi: 10.1111/cas.12087

functions or other cellular PDZ protein(s) play(s) a major role in Tax1 functions. The present study identifies MAGI-1 as a novel Tax1 interacting partner and found that Tax1 aberrantly sequesters MAGI-1 into Tax1 containing complexes and translocates it from the detergent-soluble to the detergent-insoluble cellular fraction (Figs 2,3). Since MAGI-1 is a member of the MAGUK family of proteins that function to assemble numerous cellular targets into large signaling complexes in cells,[24] these results suggest that Tax1, through mislocalizing MAGI-1, may disrupt the protein complexes and interfere with their cell signaling activities to promote aberrant cell growth of HTLV-1-infected cells.

Human T-cell leukemia virus type 1-transformed human T-cells displayed a reduced expression of MAGI-1 as compared to their HTLV-1-uninfected counterparts (Figs 6A, B). In addition, while Tax1 expression in CTLL-2 cells in the presence of IL-2 little affected MAGI-1 expression (Fig. 4B), Tax1-induced IL-2-independent transformation of CTLL-2 cells downregulated MAGI-1 expression and the downregulation was not restored by the addition of IL-2 (Figs 4C, 5A). The downregulations of MAGI-1 in Tax1-transformed cells were independent of Tax1 PBM, since Tax1ΔC-transformed cells also displayed a downregulated expression of MAGI-1 (Fig. 4C). Moreover, IL-2-independent transformation of CTLL-2 by another oncoprotein hAkt1ΔPH also downregulated MAGI-1 expression (Fig. 5B). Collectively, these results suggest that Tax1 indirectly downregulates MAGI-1 in CTLL-2 cells during the IL-2-independent transformation process. Thus, it is tempting to speculate that cells with a low MAGI-1 expression are selected during the transformation and immortalization of T-cells by Tax1 or HTLV-1.

Unlike Tax1, Tax2-immortalized human T-cells expressed substantial amounts of MAGI-1 (Fig. 6C). Our recent study showed that Tax2 immortalizes human T-cells much more efficiently than Tax1, and the difference is not mediated by the PBM,[44] indicating that a difference between Tax1 and Tax2 other than the PBM controls T-cell immortalization activities by Tax1 and Tax2. Based on these observations, we present a hypothesis to explain the distinct MAGI-1 expression in Tax1-immortalized cells versus Tax2-immortalized cells; Tax2 can immortalize both MAGI-1-high and MAGI-1-low expressing cells, whereas Tax1 can immortalize only MAGI-1-low expressing cells. Further analysis is, however, required to elucidate the mechanism underlining the differential MAGI-1 expression in Tax1- versus Tax2-immortalized cells. It should be noted that it still remains unclear as to why HTLV-1 is more pathogenic than HTLV-2; however, it has been proposed that such a difference in pathogenesity is attributed to the differences in the respective Tax activities. Our current findings add to this notion that the downregulation of MAGI-1 in Tax1-immortalized T-cells contributes to the pathogenic difference between HTLV-1 and HTLV-2.

Although the function of MAGI-1 in T-cells remains unknown, Tax1 can interfere with the activities of MAGI-1 via altering the subcellular localization and downregulating the mRNA. Further research is necessary to clarify the role of MAGI-1 in T-cell functions and more specifically in HTLV-1 pathogenesis. Nevertheless, MAGI-1 has been proposed to play tumour suppressor functions in other systems. For instance, MAGI-1 but not the related MAGI-2/3 suppressed the transformation of baby rat kidney cells by EJ-ras oncoprotein together with either HPV-16 E6 or adenovirus E1A oncoprotein.[32] Moreover, downregulation of MAGI-1 was associated with poor prognosis of hepatocellular carcinoma.[50] Two other viral oncoproteins, adenovirus-9 E4-ORF1 and high-risk HPV E6 were also shown to sequester MAGI-1 in the cytoplasm and target it for degradation, respectively.[37] It is therefore not surprising to speculate that MAGI-1 plays a tumour suppressor function in T-cells.

In summary, we report herein that similar to other viral oncoproteins, Tax1 can inactivate functions of the PDZ protein MAGI-1 by alteration of its subcellular localization and selection of cells with its downregulated mRNA expression in transformation. Since MAGI-1 has been implicated in tumour suppression in other systems, this can be as a mechanism to suppress its potential anti-tumor functions in HTLV-1-infected cells.

Acknowledgments

We appreciate Dr H. Miyoshi, Dr L. Banks, Dr R. Mahieux, Dr W. Hall and Takeda Pharmaceutical Company for providing us with the respective reagents. We also express our gratitude to Misako Tobimatsu for her technical assistance. This research was supported in part by the Ministry of Education, Science, Sports and Culture of Japan and a Grant from the Niigata University Kyowakai Society.

Disclosure Statement

The authors have no conflict of interest.

References

1 Yao J, Wigdahl B. Human T cell lymphotropic virus type I genomic expression and impact on intracellular signaling pathways during neurodegenerative disease and leukemia. *Front Biosci* 2000; **5**: D138–68.
2 Yoshida M, Miyoshi I, Hinuma Y. Isolation and characterization of retrovirus from cell lines of human adult T-cell leukemia and its implication in the disease. *Proc Natl Acad Sci USA* 1982; **79**: 2031–5.
3 Matsuoka M, Jeang KT. Human T-cell leukaemia virus type 1 (HTLV-1) infectivity and cellular transformation. *Nat Rev Cancer* 2007; **7**: 270–80.
4 Grassmann R, Aboud M, Jeang KT. Molecular mechanisms of cellular transformation by HTLV-1 Tax. *Oncogene* 2005; **24**: 5976–85.
5 Nerenberg M, Hinrichs SH, Reynolds RK, Khoury G, Jay G. The tat gene of human T-lymphotropic virus type 1 induces mesenchymal tumors in transgenic mice. *Science* 1987; **237**: 1324–9.
6 Iwanaga Y, Tsukahara T, Ohashi T *et al.* Human T-cell leukemia virus type 1 tax protein abrogates interleukin-2 dependence in a mouse T-cell line. *J Virol* 1999; **73**: 1271–7.
7 Hasegawa H, Sawa H, Lewis MJ *et al.* Thymus-derived leukemia-lymphoma in mice transgenic for the Tax gene of human T-lymphotropic virus type I. *Nat Med* 2006; **12**: 466–72.
8 Ohsugi T, Kumasaka T, Okada S, Urano T. The Tax protein of HTLV-1 promotes oncogenesis in not only immature T cells but also mature T cells. *Nat Med* 2007; **13**: 527–8.
9 Grassmann R, Berchtold S, Radant I *et al.* Role of human T-cell leukemia virus type 1× region proteins in immortalization of primary human lymphocytes in culture. *J Virol* 1992; **66**: 4570–5.
10 Akagi T, Shimotohno K. Proliferative response of Tax1-transduced primary human T cells to anti-CD3 antibody stimulation by an interleukin-2-independent pathway. *J Virol* 1993; **67**: 1211–7.
11 Robek MD, Ratner L. Immortalization of CD4(+) and CD8(+) T lymphocytes by human T-cell leukemia virus type 1 Tax mutants expressed in a functional molecular clone. *J Virol* 1999; **73**: 4856–65.
12 Rousset R, Fabre S, Desbois C, Bantignies F, Jalinot P. The C-terminus of the HTLV-1 Tax oncoprotein mediates interaction with the PDZ domain of cellular proteins. *Oncogene* 1998; **16**: 643–54.
13 Suzuki T, Ohsugi Y, Uchida-Toita M, Akiyama T, Yoshida M. Tax oncoprotein of HTLV-1 binds to the human homologue of Drosophila discs large tumor suppressor protein, hDLG, and perturbs its function in cell growth control. *Oncogene* 1999; **18**: 5967–72.
14 Hirata A, Higuchi M, Niinuma A *et al.* PDZ domain-binding motif of human T-cell leukemia virus type 1 Tax oncoprotein augments the transforming activity in a rat fibroblast cell line. *Virology* 2004; **318**: 327–36.
15 Tsubata C, Higuchi M, Takahashi M *et al.* PDZ domain-binding motif of human T-cell leukemia virus type 1 Tax oncoprotein is essential for the interleukin 2 independent growth induction of a T-cell line. *Retrovirology* 2005; **2**: 46.

16 Xie L, Yamamoto B, Haoudi A, Semmes OJ, Green PL. PDZ binding motif of HTLV-1 Tax promotes virus-mediated T-cell proliferation in vitro and persistence *in vivo*. *Blood* 2006; **107**: 1980–8.
17 Feuer G, Green PL. Comparative biology of human T-cell lymphotropic virus type 1 (HTLV-1) and HTLV-2. *Oncogene* 2005; **24**: 5996–6004.
18 Hall WW, Fujii M. Deregulation of cell-signaling pathways in HTLV-1 infection. *Oncogene* 2005; **24**: 5965–75.
19 Higuchi M, Fujii M. Distinct functions of HTLV-1 Tax1 from HTLV-2 Tax2 contribute key roles to viral pathogenesis. *Retrovirology* 2009; **6**: 117.
20 Lee SS, Weiss RS, Javier RT. Binding of human virus oncoproteins to hDlg /SAP97, a mammalian homolog of the Drosophila discs large tumor suppressor protein. *Proc Natl Acad Sci USA* 1997; **94**: 6670–5.
21 Tomaić V, Gardiol D, Massimi P, Ozbun M, Myers M, Banks L. Human and primate tumour viruses use PDZ binding as an evolutionarily conserved mechanism of targeting cell polarity regulators. *Oncogene* 2009; **28**: 1–8.
22 Kiyono T, Hiraiwa A, Fujita M, Hayashi Y, Akiyama T, Ishibashi M. Binding of high-risk human papillomavirus E6 oncoproteins to the human homologue of the Drosophila discs large tumor suppressor protein. *Proc Natl Acad Sci USA* 1997; **94**: 11612–6.
23 Craven SE, Bredt DS. PDZ proteins organize synaptic signaling pathways. *Cell* 1998; **93**: 495–8.
24 Fanning AS, Anderson JM. PDZ domains: fundamental building blocks in the organization of protein complexes at the plasma membrane. *J Clin Invest* 1999; **103**: 767–72.
25 Giallourakis C, Cao Z, Green T *et al.* A molecular-properties-based approach to understanding PDZ domain proteins and PDZ ligands. *Genome Res* 2006; **16**: 1056–72.
26 Thomas M, Laura R, Hepner K *et al.* Oncogenic human papillomavirus E6 proteins target the MAGI-2 and MAGI-3 proteins for degradation. *Oncogene* 2002; **21**: 5088–96.
27 Gardiol D, Kühne C, Glaunsinger B, Lee SS, Javier R, Banks L. Oncogenic human papillomavirus E6 proteins target the discs large tumour suppressor for proteasome-mediated degradation. *Oncogene* 1999; **18**: 5487–96.
28 Nakagawa S, Huibregtse JM. Human scribble (Vartul) is targeted for ubiquitin-mediated degradation by the high-risk papillomavirus E6 proteins and the E6AP ubiquitin-protein ligase. *Mol Cell Biol* 2000; **20**: 8244–53.
29 Javier RT. Cell polarity proteins: common targets for tumorigenic human viruses. *Oncogene* 2008; **27**: 7031–46.
30 Okajima M, Takahashi M, Higuchi M *et al.* Human T-cell leukemia virus type 1 Tax induces an aberrant clustering of the tumor suppressor Scribble through the PDZ domain-binding motif dependent and independent interaction. *Virus Genes* 2008; **37**: 231–40.
31 Senda T, Shimomura A, Iizuka-Kogo A. Adenomatous polyposis coli (Apc) tumor suppressor gene as a multifunctional gene. *Anat Sci Int* 2005; **80**: 121–31.
32 Massimi P, Gammoh N, Thomas M, Banks L. HPV E6 specifically targets different cellular pools of its PDZ domain-containing tumour suppressor substrates for proteasome-mediated degradation. *Oncogene* 2004; **23**: 8033–9.
33 Ishidate T, Matsumine A, Toyoshima K, Akiyama T. The APC-hDLG complex negatively regulates cell cycle progression from the G0/G1 to S phase. *Oncogene* 2000; **19**: 365–72.
34 Ishioka K, Higuchi M, Takahashi M *et al.* Inactivation of tumor suppressor Dlg1 augments transformation of a T-cell line induced by human T-cell leukemia virus type 1 Tax protein. *Retrovirology* 2006; **3**: 71.
35 Dobrosotskaya I, Guy RK, James GL. MAGI-1, a membrane-associated guanylate kinase with a unique arrangement of protein-protein interaction domains. *J Biol Chem* 1997; **272**: 31589–97.
36 Kotelevets L, van Hengel J, Bruyneel E, Mareel M, van Roy F, Chastre E. Implication of the MAGI-1b/PTEN signalosome in stabilization of adherens junctions and suppression of invasiveness. *FASEB J* 2005; **19**: 115–7.
37 Glaunsinger BA, Lee SS, Thomas M, Banks L, Javier R. Interactions of the PDZ-protein MAGI-1 with adenovirus E4-ORF1 and high-risk papillomavirus E6 oncoproteins. *Oncogene* 2000; **19**: 5270–80.
38 Kranjec C, Banks L. A systematic analysis of human papillomavirus (HPV) E6 PDZ substrates identifies MAGI-1 as a major target of HPV type 16 (HPV-16) and HPV-18 whose loss accompanies disruption of tight junctions. *J Virol* 2011; **85**: 1757–64.
39 Yoshita M, Higuchi M, Takahashi M, Oie M, Tanaka Y, Fujii M. Activation of mTOR by human T-cell leukemia virus type 1 Tax is important for the transformation of mouse T cells to interleukin-2-independent growth. *Cancer Sci* 2012; **2**: 369–74.
40 Endo K, Hirata A, Iwai K *et al.* Human T-cell leukemia virus type 2 (HTLV-2) Tax protein transforms a rat fibroblast cell line but less efficiently than HTLV-1 Tax. *J Virol* 2002; **76**: 2648–53.
41 Higuchi M, Tsubata C, Kondo R *et al.* Cooperation of NF-kappaB2/p100 activation and the PDZ domain binding motif signal in human T-cell leukemia virus type 1 (HTLV-1) Tax1 but not HTLV-2 Tax2 is crucial for interleukin-2-independent growth transformation of a T-cell line. *J Virol* 2007; **81**: 11900–7.
42 Tanaka Y, Yoshida A, Tozawa H, Shida H, Nyunoya H, Shimotohno K. Production of a recombinant human T-cell leukemia virus type-I trans-activator (tax1) antigen and its utilization for generation of monoclonal antibodies against various epitopes on the tax1 antigen. *Int J Cancer* 1991; **48**: 623–30.
43 Meertens L, Chevalier S, Weil R, Gessain A, Mahieux R. A 10-amino acid domain within human T-cell leukemia virus type 1 and type 2 tax protein sequences is responsible for their divergent subcellular distribution. *J Biol Chem* 2004; **279**: 43307–20.
44 Imai M, Higuchi M, Kawamura H *et al.* Human T cell leukemia virus type 2 (HTLV-2) Tax2 has a dominant activity over HTLV-1 Tax1 to immortalize human CD4(+) T cells. *Virus Genes* 2013; **46**: 39–46.
45 Ohashi M, Sakurai M, Higuchi M *et al.* Human T-cell leukemia virus type 1 Tax oncoprotein induces and interacts with a multi-PDZ domain protein, MAGI-3. *Virology* 2004; **320**: 52–62.
46 Arpin-Andre C, Mesnard JM. The PDZ domain-binding motif of the human T cell leukemia virus type 1 tax protein induces mislocalization of the tumor suppressor hScrib in T cells. *J Biol Chem* 2007; **282**: 33132–41.
47 Aoyagi T, Takahashi M, Higuchi M *et al.* The PDZ domain binding motif (PBM) of human T-cell leukemia virus type 1 Tax can be substituted by heterologous PBMs from viral oncoproteins during T-cell transformation. *Virus Genes* 2010; **40**: 193–9.
48 Ross TM, Pettiford SM, Green PL. The tax gene of human T-cell leukemia virus type 2 is essential for transformation of human T lymphocytes. *J Virol* 1996; **70**: 5194–202.
49 Pearson HB, Perez-Mancera PA, Dow LE *et al.* SCRIB expression is deregulated in human prostate cancer, and its deficiency in mice promotes prostate neoplasia. *J Clin Invest* 2011; **121**: 4257–67.
50 Zhang G, Liu T, Wang Z. Downregulation of MAGI1 associates with poor prognosis of hepatocellular carcinoma. *J Invest Surg* 2012; **25**: 93–9.

doi: 10.1111/cas.12087

Virus Genes (2013) 46:39–46
DOI 10.1007/s11262-012-0831-9

Human T cell leukemia virus type 2 (HTLV-2) Tax2 has a dominant activity over HTLV-1 Tax1 to immortalize human CD4$^+$ T cells

Michitaka Imai · Masaya Higuchi · Hiroki Kawamura · Manami Yoshita · Masahiko Takahashi · Masayasu Oie · Hideaki Matsuki · Yuetsu Tanaka · Yutaka Aoyagi · Masahiro Fujii

Received: 2 July 2012 / Accepted: 20 September 2012 / Published online: 29 September 2012

Abstract While human T cell leukemia virus type 1 (HTLV-1) is the causative agent of adult T cell leukemia, a close relative, HTLV-2, is not associated with any leukemia. HTLV-1 and HTLV-2 encode the Tax1 and Tax2 proteins, respectively, which are essential for the immortalization of human T cells by the respective viruses, thereby causing persistent infection. In this study, we compared Tax1 and Tax2 with respect to their immortalization activity in human T cells. Lentivirus-mediated transduction of the *tax2* gene into human peripheral blood mononuclear cells stimulated with phytohemagglutinin and interleukin-2 in 96-well plates induced outgrowing T cells in most wells, but the cells infected with the control viruses died within 3 weeks. Surprisingly, the number of outgrowing cells induced by Tax2 was much higher than that induced by Tax1, and the appearance of outgrowing cells by Tax2 was earlier than that induced by Tax1. Nevertheless, both Tax2 and Tax1 preferentially immortalized CD4$^+$ T cells, but not CD8$^+$ T cells. Our study showed that HTLV-2 Tax2 can immortalize human CD4$^+$ T cells, and the activity is much higher than that of Tax1. The distinct T cell immortalization activities of Tax2 and Tax1 might therefore play a role in the different pathogeneses observed for these two viruses.

Keywords HTLV-1 · HTLV-2 · Tax2 · CD4 · ATL

Introduction

Human T cell leukemia virus type 1 (HTLV-1) is the causative agent of adult T cell leukemia (ATL) [1–3]. HTLV-1 infection is generally asymptomatic throughout life, but 3–5 % of HTLV-1-infected individuals develop ATL, with an average age of onset at 60 years. These findings indicate that multiple host and environmental factors are associated with the development of the disease [4]. HTLV-1 immortalizes primary human T cells in the presence of interleukin(IL)-2 in vitro, and a fraction of cells, as a rare event, progress to acquire IL-2-independent growth properties [5, 6]. These studies suggest that the immortalization of T cells by HTLV-1 is therefore of critical importance to establish a persistent infection in vivo [7].

In addition to the structural genes, HTLV-1 has at least two oncogenic genes, *tax1* and *HBZ* (HTLV-1 bZIP factor). In transgenic mice, Tax1 and HBZ independently induce T cell lymphoma [8–10]. In addition, Tax1, but not HBZ, is essential for the immortalization of human T cells. For instance, the inactivation of the *tax1* gene in recombinant HTLV-1 abrogates the T cell immortalization activity of HTLV-1 [11].

The first two authors contributed equally to this study.

M. Imai · M. Higuchi · M. Yoshita · M. Takahashi · M. Oie · H. Matsuki · M. Fujii (✉)
Division of Virology, Niigata University Graduate School of Medical and Dental Sciences, 1-757 Asahimachi-Dori, Niigata 951-8510, Japan
e-mail: fujiimas@med.niigata-u.ac.jp

M. Imai · Y. Aoyagi
Division of Gastroenterology and Hepatology, Niigata University Graduate School of Medical and Dental Sciences, 1-757 Asahimachi-Dori, Niigata 951-8510, Japan

H. Kawamura
Department of Immunology, Niigata University Graduate School of Medical and Dental Sciences, 1-757 Asahimachi-Dori, Niigata 951-8510, Japan

Y. Tanaka
Department of Immunology, Graduate School and Faculty of Medicine, University of the Ryukyus, Okinawa, Japan

Moreover, the transduction of the *tax1* gene without other viral genes into primary peripheral blood mononuclear cells (PBMC) establishes immortalized T cells [12, 13].

HTLV-2 is a close relative of HTLV-1, and it also immortalizes human T cells with equivalent efficiency to HTLV-1 [14]. Nevertheless, there is no etiological association of HTLV-2 with malignancies. Therefore, comparative studies between HTLV-1 and HTLV-2 provide insight into the molecular mechanism of HTLV-1 leukemogenesis. To obtain information about the distinct pathogenesis between HTLV-1 and HTLV-2, we investigated whether HTLV-2 Tax2 can immortalize human T cells, and how strong (relative to Tax1) the effects of Tax2 are on immortalizing human T cells. We found that Tax2 can immortalize T cells in vitro, and surprisingly, that the activity was much higher than that of Tax1. These findings will be discussed in the context of the distinct pathogenesis between HTLV-1 and HTLV-2.

Materials and methods

Cells and culture conditions

Jurkat and SLB-1 cells are HTLV-1-negative and HTLV-1-positive human T cell lines, respectively. These T cell lines were cultured in RPMI1640 medium supplemented with 10 % fetal bovine serum (FBS), 4 mM glutamine, penicillin (100 U/ml), and streptomycin (100 μg/ml) (RPMI/10 %FBS). The 293T cells were derived from a human kidney, and the cells were cultured in Dulbecco's modified Eagle medium supplemented with 10 % FBS, 4 mM glutamine, 0.1 mM MEM non-essential amino acids (aa), penicillin (100 U/ml), and streptomycin (100 μg/ml).

Plasmids

CSII-EF-EGFP, CSII-EF-Tax1, CSII-EF-Tax2B, and CSII-EF-Tax300 are the lentiviral expression vectors encoding EGFP, Tax1, Tax2B, and Tax300, respectively [15–17]. CSII-EF-IG is a lentiviral bicistronic EGFP expression vector and was also used for Tax gene expression [16]. pEFneoTax1, pEFneoTax2B, and pEFneoTax300 were used as the expression vectors encoding Tax1, Tax2B, and Tax300, respectively [16, 17]. The *tax* mutant gene, *tax300*, is a chimeric gene that contains the N-terminal region of Tax2B from aas 1 to 299 and the C-terminal region of Tax1 from aa 300 to 353. *tax300* is the same gene as *tax221* which was described in a previous study [18]. pNFAT-Luc is a luciferase expression plasmid that is regulated by three copies of the NFAT site (−286 to −249 of human IL-2 gene) and the human IL-2 promoter (−64 to −47) [19]. The κB-Luc is a luciferase expression plasmid regulated by the κB element of the IL-2 receptor α-chain gene and the minimal HTLV-1 promoter [20]. pGK/β-gal expresses β-galactosidase under the control of the phosphoglycerate kinase promoter and is used to normalize the transfection efficiency.

Immortalization assay

Human PBMCs were isolated from the blood of a healthy donor. They were stimulated with 10 μg/ml phytohemagglutinin (PHA) (Sigma Aldrich) in RPMI/20 %FBS supplemented with 55 μM 2-mercaptoethanol (2-ME) for 2 days and then further cultured in RPMI/20 %FBS with 0.5 nM IL-2 and 2-ME for 2 days. To generate recombinant lentiviruses, 293T cells were transfected with pCAG-HIVgp, pCMV-VSV-G-RSV-Rev (provided by Dr. H. Miyoshi, RIKEN Tsukuba Institute) and the respective lentiviral vectors encoding Tax1, Tax2B, or Tax300 using FuGENE 6 (Roche). At 72 h after the transfection, the supernatant was collected and used to infect PHA-stimulated PBMC (4×10^5 cells) in a final volume of 1 ml of RPMI/20 %FBS containing 8 μg/ml polybrene, 0.5 nM IL-2, and 2-ME. The virus titer was measured by a Lenti-X qRT-PCR Titration Kit (Clontech), and the viruses containing 1.2×10^8 copies of viral genomic RNA were used for the infection. At 48 h after the infection, the cells were resuspended in RPMI/20 %FBS with IL-2 and 2-ME and cultured in 96-well flat-bottom plates at the density of 1.33×10^3 cells/0.1 ml/well, 4.0×10^3 cells/0.1 ml/well, or 1.2×10^4 cells/0.1 ml/well for 10 weeks. Half of the volume of culture medium was exchanged with new medium once every 4–5 days. The number of wells containing outgrowing cells was counted by light microscopy.

Western blotting analysis

To prepare total cell extracts, the cells were lysed in sodium dodecyl sulfate (SDS) sample buffer (2 % SDS, 62.5 mM Tris–HCl pH 6.8, 10 % glycerol, 50 mM dithiothreitol, 0.01 % bromophenol blue) and heated at 95 °C for 5 min. Then they were size-separated by electrophoresis under reducing conditions in 10 % polyacrylamide gel with SDS. The proteins in the gel were electrotransferred onto a polyvinylidene difluoride membrane (Bio-Rad Laboratories). The membrane was incubated with TBS-T [20 mM Tris–HCl (pH 7.4), 150 mM NaCl, and 0.1 % Tween 20] in 5 % skimmed milk for 1 h at room temperature to inhibit non-specific binding and was further incubated with either an anti-Tax1 mouse monoclonal antibody (Taxy-7) [21] or rabbit anti-Tax2 polyclonal serum (GP3738) [22]. After being washed with TBS-T, the membranes were incubated with either anti-mouse (for Tax1) or anti-rabbit (for Tax2) immunoglobulin G

conjugated with horseradish peroxidase (Bio-Rad Laboratories). Protein bands in the membrane recognized by the antibodies were visualized using the ECL Western blotting detection system (GE Healthcare).

Flow cytometric analysis

The cells were incubated with phycoerythrin (PE)-labeled anti-human CD4 and fluorescein isothiocyanate (FITC)-labeled anti-human CD8 monoclonal antibodies or with isotype matched control antibodies for 30 min at 4 °C. After washing with PBS containing 2 % FBS, the cells were analyzed by flow cytometer (FACScan, Becton–Dickinson) using the Cellquest software program (Becton–Dickinson). PE-labeled mouse anti-human CD8 and FITC-labeled anti-CD4 were purchased from eBioscience.

Transient transfection and luciferase assays

Jurkat cells in RPMI/10 %FBS were seeded at 2×10^5 cells/1.0 ml/well in a 12-well plate. The cells then were cotransfected with the Tax expression plasmid and pGK/β-gal, together with either pNFAT-Luc or κB-Luc by using TransFectin (Bio-Rad Technologies) according to the manufacturer's instructions. At 48 h after transfection, the cell lysates were harvested, and the luciferase and β-galactosidase activities in the lysates were determined using a Luciferase assay system (Promega) and Galacto-Light System (Applied Biosystems). The activity of luciferase was normalized to that of β-galactosidase. The assay was carried out three times to confirm the reproducibility.

Measurement of nuclear NFATc2 and NF-κB p65 proteins

NE-PER nuclear and cytoplasmic extraction reagents (Thermo Scientific) were used to prepare cytoplasmic and nuclear fractions from Tax-immortalized cells and Jurkat cells. The cytoplasmic (10 μg) and the nuclear (5 μg) fractions were characterized by a Western blotting analysis using anti-p65 (F6; Santa Cruz Biotechnology), anti-NFATc2 (4G6-G5; Santa Cruz Biotechnology), anti-Sp1 (PEP2; Santa Cruz Biotechnology), anti-Tubulin (DM1A; Calbiochem), and anti-Tax1 and anti-Tax2 antibodies.

Results

Tax2 immortalizes primary human T cells in the presence of IL-2

The tax2B gene used in this study was derived from the HTLV-2b subtype [15]. The tax300 gene is a chimeric gene that combines tax2B and tax1, and has the N-terminal Tax2B aa (1–299) and the C-terminal Tax1 aa (300–353) (Fig. 1a) [16]. To measure the immortalization activity of the genes in human T cells, we generated lentivirus vectors encoding tax2B, tax300, and tax1 by using 293T cells, and the virus titers in the culture supernatant of 293T cells were adjusted by quantification of the viral genome by real time polymerase chain reaction (PCR). The viruses containing 1.2×10^8 copies of viral genomic RNA were then used to infect two types of cells, human PBMCs stimulated with 10 μg PHA and recombinant IL-2 for 2 days, or a human T cell line (Jurkat). The control lentivirus expressed green fluorescent protein (GFP). The anti-Tax1 antibody detected Tax1 and Tax300 proteins, but not Tax2B, in both PBMCs and Jurkat cells infected with the respective viruses, although the expression level in PBMCs was lower than in Jurkat cells (Fig. 1b, c). An anti-Tax2 antibody detected all three Tax proteins in both cells. However, it should be noted that the anti-Tax2 antibody was raised against Tax2 peptides, and detects Tax2 and Tax300 proteins more efficiently than Tax1 protein [16, 22]. On the other hand, anti-Tax1 antibody detects Tax1 and Tax300 proteins more efficiently than Tax2B protein. Collectively, the results of the Western blotting analyses indicated that the amounts of Tax2B, Tax1, and Tax300 proteins in PBMCs infected with the respective viruses were either almost equivalent or the

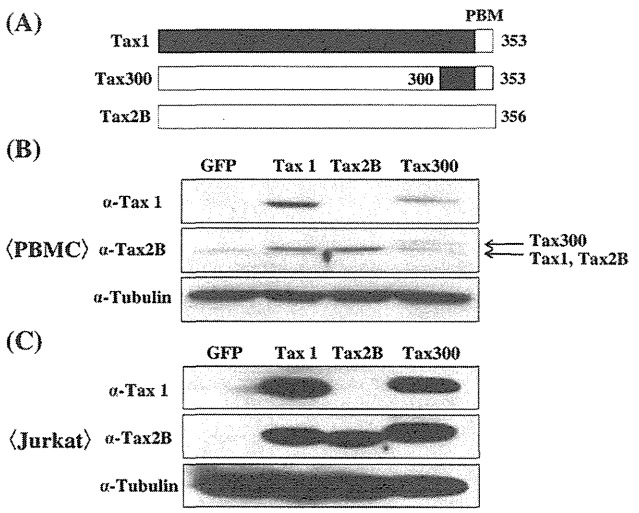

Fig. 1 Lentiviral introduction of *tax1*, *tax2B*, and *tax300* into PBMCs and Jurkat. **a** Tax1 and Tax2B consisted of 353 and 356 aa, respectively. Tax300 has the N-terminal region of Tax2B from aa 1 to 299 and the C-terminal region of Tax1 from aa 300 to 353. PBM indicates the PDZ domain binding motif present only in Tax1 but not in Tax2B, which is essential for the augmented transforming activity of Tax1 in CTLL-2 relative to Tax2 [32, 34]. **b**, **c** The PHA-stimulated PBMCs (**b**) and Jurkat cells (**c**) were infected with the indicated viruses. At 48 h after the infection, the cell lysates were prepared, and the amounts of Tax1, Tax2B, Tax300, and Tubulin in the lysates were measured by a Western blotting analysis using anti-Tax1 (Taxy-7), Tax2, and anti-Tubulin antibodies

amount of Tax1 was more than that of Tax2B. Tax300 was always detected as a higher molecular protein than Tax1 by our Western blotting analysis, although both Tax300 and Tax1 consist of 353 aas. This difference between Tax300 and Tax1 might be caused by their distinct conformation or distinct post-translational modification.

Next, these virus-infected PBMCs were cultured in the presence of IL-2 in a 96-well plate at cell densities of 1.2×10^4, 4×10^3, and 1.33×10^3 cells/well (Fig. 2a, b). At 7- to 10-days post-infection, PBMCs that were infected with Tax2B-viruses showed multiple small clumps of cells in all the wells, and the number of clumps was much higher than that of the cells infected with the control virus. Thereafter, these Tax2B-infected cells continuously proliferated, and 80 out of 96 wells (1.2×10^4 cells/well) contained obvious outgrowing cells at 10-weeks post-infection, whereas all the cells infected with the control virus had died within 3 weeks. At 7- to 10-days post-infection, Tax1 also induced small clumps of cells similar to Tax2B in all the wells, but they then stopped proliferating for 4–5 weeks. Thereafter, some cells started to regrow, and at 10-weeks post-infection, 10 out of 96 wells contained obvious outgrowing cells. Tax300 also induced outgrowing cells from PBMCs, and at 12-weeks post-infection, 36 out of 96 wells contained obvious outgrowing cells, the number of which was lower than that induced by Tax2B. Three independent experiments confirmed the augmented immortalization activity of Tax2B relative to Tax1. We transferred several outgrowing cells to a 24-well plate, and then to a culture flask, and the expression levels of Tax in such cells were characterized by a Western blotting analysis. Three Tax2B-transduced cells express the Tax2B protein, but not Tax1, whereas three Tax1-transduced cells expressed Tax1 protein, but not Tax2B (Fig. 2c). These results indicated that Tax2 is therefore able to immortalize PBMCs, and this activity is stronger than that of Tax1.

Tax1 preferentially immortalizes $CD4^+$ T cells [12, 23]. Therefore, it would be interesting to see whether Tax2 also has

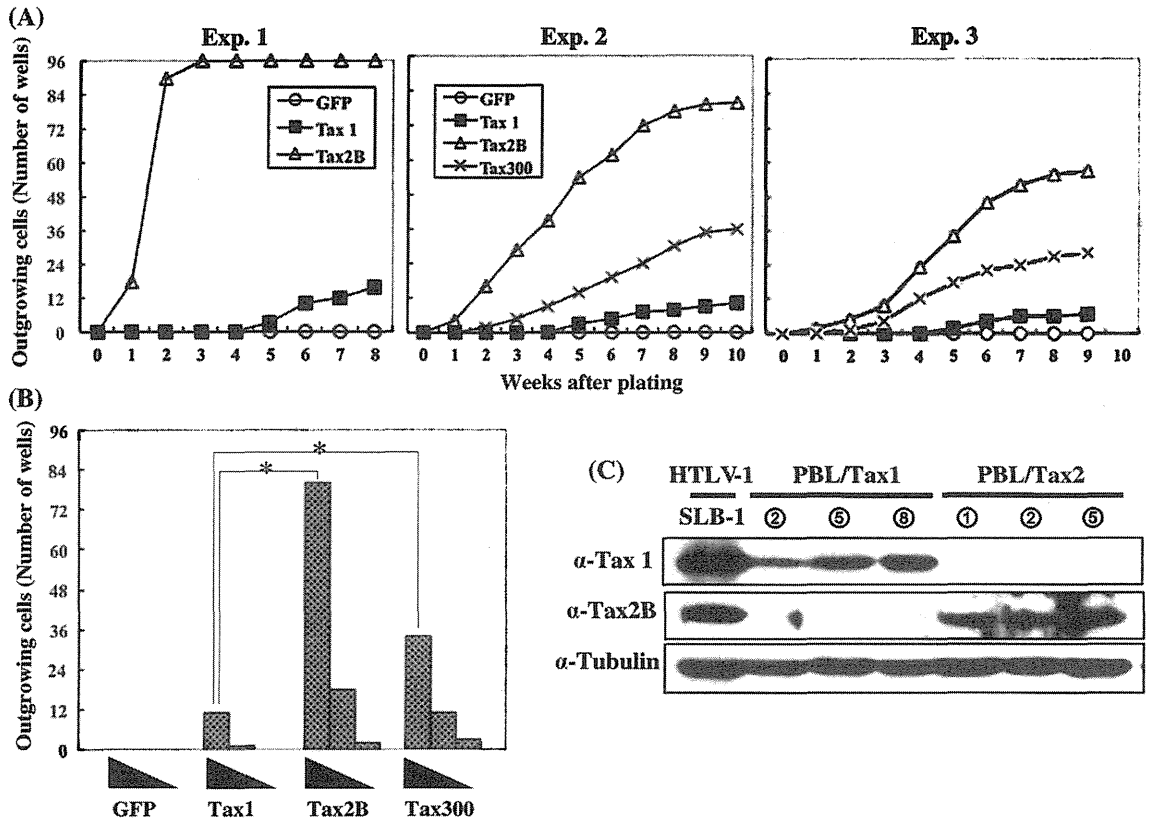

Fig. 2 Tax2B immortalizes human PBMCs. **a**, **b** PHA-stimulated PBMCs infected with lentiviruses encoding *GFP*, *tax1*, *tax2B*, or *tax300* were cultured in RPMI/20 %FBS/IL-2 in 96-well plates at a density of 1.2×10^4, 4.0×10^3, or 1.33×10^3 cells/0.1 ml/well for 10 weeks. The number of wells containing outgrowing cells (seeded at cell density of 1.2×10^4 cells/0.1 ml/well) was counted under a light microscope for 8–10 weeks. The results of three independent experiments are presented in **a**. The number of wells containing outgrowing cells (seeded at cell density of 1.2×10^4, 4.0×10^3, or 1.33×10^3 cells/0.1 ml/well) at 10-weeks post-infection of the experiment 2 in **a** is indicated in **b**. *Asterisk* A significant difference ($p < 0.001$) by the χ^2 test. **c** Three PBL/Tax1 cell lines (PBL/Tax1-2, PBL/Tax1-5, PBL/Tax1-8) and three PBL/Tax2B cell lines (PBL/Tax2B-1, PBL/Tax2B-2, PBL/Tax2B-5) were established from the PBMCs infected with Tax1 and Tax2B lentiviruses as shown above, respectively. The amounts of Tax1 and Tax2B protein in these cells were measured by a Western blotting analysis using anti-Tax1 and Tax2 antibodies

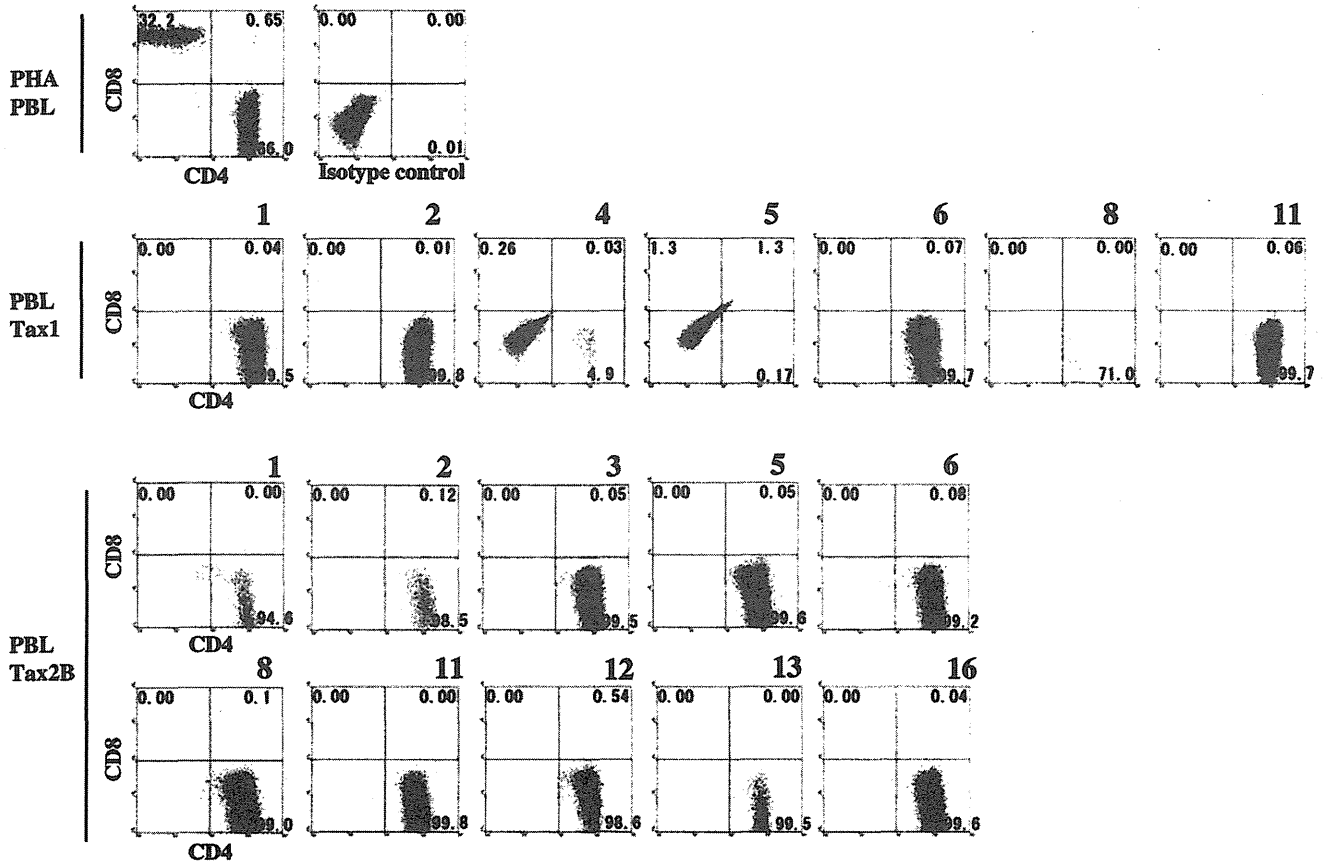

Fig. 3 Tax-immortalized cells express CD4, but not CD8 antigen. The Tax-immortalized T cell lines were characterized for CD4 and CD8 expression using a flow cytometer. Seven PBL/Tax1 cell lines and ten PBL/Tax2B cell lines were established by infection of PBMCs with the Tax1-lentivirus or Tax2B-lentivirus, respectively, and were cultured in the presence of IL-2

an immortalization ability similar to that of Tax1. A flow cytometric analysis showed that all ten Tax2B-immortalized cells were CD4 single positive (Fig. 3). On the other hand, five out of the seven Tax1-immortalized cells were CD4 single positive, one was double negative and the last one (PBL/Tax1-4) was a mixture of double negative cells with a minor population of CD4 single positive cells. These results indicated that Tax2 immortalizes $CD4^+$ T cells, but not $CD8^+$ T cells.

Tax2 activates NFAT-dependent transcription much more efficiently than Tax1

NF-κB and NFAT are transcription factors that control the expression of many genes regulating T cell functions, including cell proliferation and anti-apoptosis, and they are stimulated by both Tax1 and Tax2 [6, 24]. To determine whether the high immortalization activity of Tax2B is related to activation of these transcription factors, we next measured the transcriptional activation by Tax2B, Tax1, and Tax300. The tax expression plasmids and luciferase reporter plasmid under the control of either NF-κB or NFAT were transfected into Jurkat cells using the lipofection method. At 48 h post-transfection, the cell lysates were prepared, and the luciferase activities were measured. Tax2B and Tax300 activated the NF-κB reporter 20- to 25-fold more than the control plasmid, and the activities were half that of Tax1 (Fig. 4). While Tax2B and Tax300 activated the NFAT reporter more than 100-fold, Tax1 only activated NFAT 3- to 10-fold. These results were consistent with those of a previous study [18]. We also examined whether Tax stimulates the nuclear localization of NF-κB p65 and NFATc2, which would indicate the activation of these transcription factors (Fig. 5a). The treatment of Jurkat cells with 12-*O*-tetradecanoylphorbol-13-acetate (TPA) and ionomycin induced an increased nuclear expression of NF-κB p65 and NFATc2 proteins. The transient transduction of Tax1 and Tax2B into Jurkat cells also induced an increased nuclear expression of NF-κB p65 and NFATc2 relative to the control, but the amount of nuclear NFATc2 in Tax1-transduced cells was lower than that of Tax2B-transduced cells, which is consistent with the above described reporter assay.

We then examined the status of NF-κB and NFAT in Tax-immortalized T cells. The amounts of nuclear p65 and NFATc2 in each of three Tax1- and Tax2B-immortalized T cells were more than those of unstimulated Jurkat and they

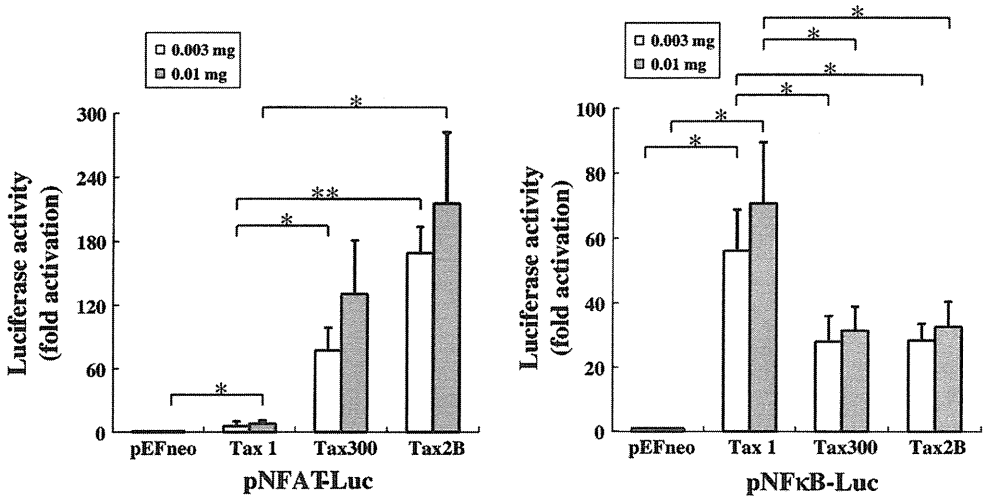

Fig. 4 Tax2B activates both NFAT and NF-κB in a T cell line. Jurkat cells (2×10^5 cells/1.0 ml/well) in a 12-well plate were co-transfected with the Tax expression plasmid and pGK/β-gal, together with either pNFAT-Luc or κB-Luc, using TransFectin. At 48 h after transfection, the luciferase and β-galactosidase activities in the lysates were determined using a luminometer. The activity of luciferase was normalized to that of β-galactosidase, and the fold activations were calculated as the ratio to that of the control transfection with the pEFneo plasmid. The data shown are the averages of three independent experiments with standard deviations. *One asterisk* and *two asterisks* indicate significant differences ($p < 0.05$) and ($p < 0.01$) by the unpaired student's *t* test, respectively

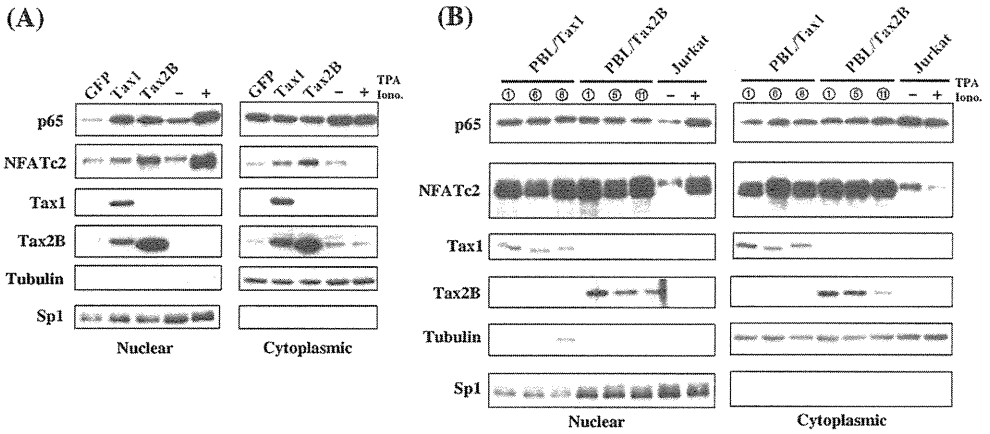

Fig. 5 Tax2B induces the nuclear translocation of NFATc2 and p65 in T cells. **a**, **b** Jurkat cells (4×10^5 cells) were infected with bicistranic Tax1-EGFP lentivirus, Tax2B-EGFP lentivirus or the control virus in 6-well plate and were cultured for 48 h. Jurkat cells (2×10^6 cells) were treated with 20 ng/ml TPA and 1 μM ionomycin for 60 min. Cytoplasmic and nuclear fractions from the infected Jurkat cells (**a**) and Tax-immortalized cells (**b**) were analyzed by a Western blotting analysis using anti-p65, anti-NFATc2, anti-Tax1, anti-Tax2B, anti-Tubulin, and anti-Sp1 antibodies. Tubulin and Sp1 were used as marker proteins that localize in the cytoplasm and the nucleus, respectively

were also equivalent to that of stimulated Jurkat, thus suggesting that Tax1- and Tax2B-immortalized cells have augmented p65- and NFATc2-dependent transcriptional activities. However, it should be noted that the high levels of nuclear NFATc2 in Tax1-immortalized T cells were unexpected, as Tax1 showed a much lower NFAT transcriptional activity than that of Tax2B (Figs. 4b, 5a). Collectively, these results suggested that Tax1- and Tax2B-immortalized T cells have equivalent activations of NF-κB p65 and NFATc2, which did not support the possibility that NFAT contributes to the distinct immortalization activity of Tax2B versus Tax1.

Discussion

In this study, we demonstrated that the HTLV-2b Tax2B protein has an immortalizing activity in human T cells within PBMCs, and such cells could be long-term cultured for at least 3 months (Fig. 2). A previous study showed that

tax2-inactivated HTLV-2 does not immortalize human T cells [25]. Taken together, these findings indicate that Tax2 is a crucial factor required for the immortalization of HTLV-2-infected T cells, thereby leading to persistent infection.

HTLV-2 and HTLV-1 preferentially immortalize $CD8^+$ T cells and $CD4^+$ T cells, respectively, in vitro [26]. Nevertheless, Tax2B selectively immortalized $CD4^+$ T cells, but not $CD8^+$ T cells, in this study (Fig. 3). These results indicate that Tax2 is not a determinant for the immortalization tropism of HTLV-2. Indeed, the chimeric virus composed of HTLV-2 and HTLV-1 showed that the *envelope* gene, but not *tax2*, is a determinant for the selective immortalization of $CD8^+$ T cells by HTLV-2 [27].

The immortalization activity of Tax2B on human T cells was much more efficient than that of Tax1 (Fig. 2). A microscopic examination revealed that Tax1 and Tax2 initially induce the outgrowth of PBMCs for 1 week. Thereafter, while the Tax2-transduced cells continue to grow, Tax1-transduced cells stop growing for several weeks, and then some cells start to regrow. The overexpression of Tax1 in several cell types, including a T cell line, was shown to induce senescence and/or cell cycle arrest [28, 29]. Therefore, such growth inhibitory activity of Tax1 might explain why Tax1-infected PBMCs stop growing for a while in culture. Tax2 might not have these growth inhibitory activities, thereby inducing greater immortalization activity in T cells than Tax1. It should be noted that HTLV-1 HBZ, which shows an oncogenic activity in transgenic mice, alleviates the growth inhibitory activity of Tax1 [10, 29]. Collectively, we herein present a hypothesis that Tax2 alone is sufficient to immortalize T cells by HTLV-2, whereas both Tax1 and HBZ are required to efficiently immortalize T cells by HTLV-1.

The same set of the lentiviruses used here previously showed that Tax1 induces IL-2-independent growth transformation to the originally IL-2-dependent T cell line, CTLL-2, and that the activity was much higher than that of Tax2B and Tax300 [16, 20]. Therefore, it was intriguing that Tax2 and Tax1 have such distinct activities to T cells in the absence and presence of IL-2, despite the fact that they originated from the common ancestor virus. One possible scenario is that Tax2 in the context of HTLV-2 has evolved to immortalize T cells in the presence of a relatively high amount of IL-2, whereas Tax1 in the context of HTLV-1 has evolved to do so in a relatively low amount of IL-2 [30]. A further analysis, however, will be required to establish this hypothesis and to determine how these differences are associated with the leukemogenic activity of HTLV-1.

In addition to NF-κB and NFAT, Tax1 activates the transcription of several cellular genes through the transcription factor CREB, and Rosin et al. [31] presented an evidence that the activation of CREB pathway by Tax1 is important for the immortalization of primary human T cells by Tax1. However, the CREB pathway is unlikely to be a main factor for the reduced immortalization activity of Tax1 relative to Tax2B, as Tax1 and Tax2B showed equivalent CREB activities in a luciferase reporter assay [18]. It should be noted that Tax1 and Tax300, but not Tax2B, have a PDZ domain binding motif (PBM) at their C-terminus (Fig. 4a), and this motif is critical for the high transforming activity of Tax1 to CTLL-2 [32]. However, Xie et al. [33] showed that the deletion of PBM in recombinant HTLV-1 minimally affects immortalization activity to human T cells in the presence of IL-2. Therefore, this motif is unlikely to be responsible for distinct immortalization activities of Tax1 and Tax2B in human T cells. Tax1 and Tax2B have other distinctions from PBM. For instance, Tax1 but neither Tax2B nor Tax300 activates the non-canonical NF-κB2 pathway, which also plays a critical role in the high transforming activity toward CTLL-2 [16, 17]. Therefore, precise comparisons of Tax1 and Tax2B including these differences are required to identify the function(s) responsible for immortalization of human T cells as well as the pathogenesis.

Acknowledgments We would like to thank Dr. Hiroyuki Miyoshi at RIKEN Tsukuba Institute for providing the lentivirus plasmids, and Dr. Renaud Mahieux and Dr. William Hall for providing the anti-Tax2 antibody and *tax2B* gene, respectively. We also wish to thank the Takeda Pharmaceutical Company for providing recombinant human IL-2. We would like to express our gratitude to Misako Tobimatsu for the excellent technical assistance. This study was supported in part by a Grant-in-Aid for Scientific Research on Priority Areas and for Scientific Research (C) of Japan, as well as a Grant for the Promotion of Niigata University Research Projects.

References

1. T. Uchiyama, J. Yodoi, K. Sagawa, K. Takatsuki, H. Uchino, Blood **50**(3), 481–492 (1977)
2. B.J. Poiesz, F.W. Ruscetti, A.F. Gazdar, P.A. Bunn, J.D. Minna, R.C. Gallo, Proc Natl Acad Sci USA **77**(12), 7415–7419 (1980)
3. Y. Hinuma, H. Komoda, T. Chosa, T. Kondo, M. Kohakura, T. Takenaka, M. Kikuchi, M. Ichimaru, K. Yunoki, I. Sato, R. Matsuo, Y. Takiuchi, H. Uchino, M. Hanaoka, Int. J. Cancer **29**(6), 631–635 (1982)
4. M. Matsuoka, K. T. Jeang, Oncogene 30(12), 1379–1389 (2011)
5. I. Miyoshi, I. Kubonishi, S. Yoshimoto, T. Akagi, Y. Ohtsuki, Y. Shiraishi, K. Nagata, Y. Hinuma, Nature **294**(5843), 770–771 (1981)
6. W.W. Hall, M. Fujii, Oncogene **24**(39), 5965–5975 (2005)
7. P. Miyazato, J. Yasunaga, Y. Taniguchi, Y. Koyanagi, H. Mitsuya, M. Matsuoka, J. Virol. **80**(21), 10683–10691 (2006)
8. H. Hasegawa, H. Sawa, M.J. Lewis, Y. Orba, N. Sheehy, Y. Yamamoto, T. Ichinohe, Y. Tsunetsugu-Yokota, H. Katano, H. Takahashi, J. Matsuda, T. Sata, T. Kurata, K. Nagashima, W.W. Hall, Nat. Med. **12**(4), 466–472 (2006)
9. T. Ohsugi, T. Kumasaka, S. Okada, T. Urano, Nat. Med. **13**(5), 527–528 (2007)

10. Y. Satou, J. Yasunaga, T. Zhao, M. Yoshida, P. Miyazato, K. Takai, K. Shimizu, K. Ohshima, P.L. Green, N. Ohkura, T. Yamaguchi, M. Ono, S. Sakaguchi, M. Matsuoka, PLoS Pathog. **7**(2), e1001274 (2011)
11. M.D. Robek, L. Ratner, J. Virol. **73**(6), 4856–4865 (1999)
12. R. Grassmann, S. Berchtold, I. Radant, M. Alt, B. Fleckenstein, J.G. Sodroski, W.A. Haseltine, U. Ramstedt, J. Virol. **66**(7), 4570–4575 (1992)
13. T. Akagi, K. Shimotohno, J. Virol. **67**(3), 1211–1217 (1993)
14. V.S. Kalyanaraman, M.G. Sarngadharan, M. Robert-Guroff, I. Miyoshi, D. Golde, R.C. Gallo, Science **218**(4572), 571–573 (1982)
15. M.J. Lewis, P. Novoa, R. Ishak, M. Ishak, M. Salemi, A.M. Vandamme, M.H. Kaplan, W.W. Hall, Virology **271**(1), 142–154 (2000)
16. M. Higuchi, C. Tsubata, R. Kondo, S. Yoshida, M. Takahashi, M. Oie, Y. Tanaka, R. Mahieux, M. Matsuoka, M. Fujii, J. Virol. **81**(21), 11900–11907 (2007)
17. T. Shoji, M. Higuchi, R. Kondo, M. Takahashi, M. Oie, Y. Tanaka, Y. Aoyagi, M. Fujii, Retrovirology **6**, 83 (2009)
18. A. Niinuma, M. Higuchi, M. Takahashi, M. Oie, Y. Tanaka, F. Gejyo, N. Tanaka, K. Sugamura, L. Xie, P.L. Green, M. Fujii, J. Virol. **79**(18), 11925–11934 (2005)
19. J.P. Northrop, K.S. Ullman, G.R. Crabtree, J. Biol. Chem. **268**(4), 2917–2923 (1993)
20. K. Endo, A. Hirata, K. Iwai, M. Sakurai, M. Fukushi, M. Oie, M. Higuchi, W.W. Hall, F. Gejyo, M. Fujii, J. Virol. **76**(6), 2648–2653 (2002)
21. Y. Tanaka, A. Yoshida, H. Tozawa, H. Shida, H. Nyunoya, K. Shimotohno, Int. J. Cancer **48**(4), 623–630 (1991)
22. L. Meertens, S. Chevalier, R. Weil, A. Gessain, R. Mahieux, J. Biol. Chem. **279**(41), 43307–43320 (2004)
23. T. Akagi, H. Ono, H. Nyunoya, K. Shimotohno, Oncogene **14**(17), 2071–2078 (1997)
24. S.C. Sun, S. Yamaoka, Oncogene **24**(39), 5952–5964 (2005)
25. T.M. Ross, S.M. Pettiford, P.L. Green, J. Virol. **70**(8), 5194–5202 (1996)
26. J. Ye, L. Xie, P.L. Green, J. Virol. **77**(14), 7728–7735 (2003)
27. L. Xie, P.L. Green, J. Virol. **79**(23), 14536–14545 (2005)
28. M. Liu, L. Yang, L. Zhang, B. Liu, R. Merling, Z. Xia, C.Z. Giam, J. Virol. **82**(17), 8442–8455 (2008)
29. H. Zhi, L. Yang, Y.L. Kuo, Y.K. Ho, H.M. Shih, C.Z. Giam, PLoS Pathog. **7**(4), e1002025 (2011)
30. M. Higuchi, M. Fujii, Retrovirology **6**, 117 (2009)
31. O. Rosin, C. Koch, I. Schmitt, O.J. Semmes, K.T. Jeang, R. Grassmann, J. Biol. Chem. **273**(12), 6698–6703 (1998)
32. C. Tsubata, M. Higuchi, M. Takahashi, M. Oie, Y. Tanaka, F. Gejyo, M. Fujii, Retrovirology **2**, 46 (2005)
33. L. Xie, B. Yamamoto, A. Haoudi, O.J. Semmes, P.L. Green, Blood **107**(5), 1980–1988 (2006)
34. A. Hirata, M. Higuchi, A. Niinuma, M. Ohashi, M. Fukushi, M. Oie, T. Akiyama, Y. Tanaka, F. Gejyo, M. Fujii, Virology **318**(1), 327–336 (2004)

MCB
Journals.ASM.org

Stress Granules Inhibit Apoptosis by Reducing Reactive Oxygen Species Production

Masahiko Takahashi, Masaya Higuchi, Hideaki Matsuki, Manami Yoshita, Toshiaki Ohsawa, Masayasu Oie, Masahiro Fujii
Division of Virology, Niigata University Graduate School of Medical and Dental Sciences, Niigata, Japan

Cells can undergo two alternative fates following exposure to environmental stress: they either induce apoptosis or inhibit apoptosis and then repair the stress-induced alterations. These processes minimize cell loss and prevent the survival of cells with aberrant DNA and protein alterations. These two alternative fates are partly controlled by stress granules (SGs). While arsenite, hypoxia, and heat shock induce the formation of SGs that inhibit apoptosis, X-ray irradiation and genotoxic drugs do not induce SGs, and they are more prone to trigger apoptosis. However, it is unclear precisely how SGs control apoptosis. This study found that SGs suppress the elevation of reactive oxygen species (ROS), and this suppression is essential for inhibiting ROS-dependent apoptosis. This antioxidant activity of SGs is controlled by two SG components, GTPase-activating protein SH3 domain binding protein 1 (G3BP1) and ubiquitin-specific protease 10 (USP10). G3BP1 elevates the steady-state ROS level by inhibiting the antioxidant activity of USP10. However, following exposure to arsenite, G3BP1 and USP10 induce the formation of SGs, which uncovers the antioxidant activity of USP10. We also found that the antioxidant activity of USP10 requires the protein kinase activity of ataxia telangiectasia mutated (ATM). This work reveals that SGs are critical redox regulators that control cell fate under stress conditions.

Upon exposure to environmental stress, cells select two distinct fates: they either induce apoptosis or inhibit apoptosis and repair any stress-induced alterations. These processes prevent the survival of cells with DNA and protein aberrations and simultaneously minimize cell loss. These cell fate decisions are partly dependent on the type of stress. While arsenite, hypoxia, and heat shock induce the formation of stress granules (SGs) that inhibit apoptosis, genotoxins and X-ray irradiation do not induce SGs, thereby making cells more prone to undergo apoptosis (1, 2). Thus, SGs are a crucial defense mechanism against environmental stress. However, the precise mechanism underlying how SGs inhibit apoptosis has not been elucidated.

SGs are cytoplasmic RNA granules, and their formation is associated with the inhibition of translation initiation and the disassembly of polysomes (3). During stress, SGs act as storage sites of nontranslating mRNAs separated from disassembled polysomes. The mRNA composition of SGs is selective; they contain mRNAs encoding housekeeping genes but exclude those encoding stress-induced genes, such as the genes encoding heat shock proteins (4). This selective storage of mRNAs by SGs promotes the translation of stress-responsive genes, thereby driving recovery from a stress.

In addition to RNAs, SGs contain various proteins, including GTPase-activating protein SH3 domain binding protein 1 (G3BP1) (5), T-cell-restricted intracellular antigens 1 (TIA-1), T-cell-restricted intracellular antigen-related protein (TIAR) (6), poly(A)-binding protein (PABP) (6), RACK1 (1), and histone deacetylase 6 (HDAC6) (7). Although the respective roles of these proteins in SG-associated functions have not yet been fully elucidated, G3BP1 has been shown to play a critical role in the assembly of SGs (5, 7, 8). G3BP1 is an RNA-binding protein, and it is localized at polysomes under steady-state conditions. Upon exposure to stress, G3BP1 forms a multimer, which initiates the assembly of SGs.

G3BP1 has been shown to regulate the stability and translation of several mRNAs. For instance, G3BP1 inhibits the translation of the mitochondrial H^+-ATP synthase subunit beta by interacting with the 3′ untranslated region of RNA (9). In addition, G3BP1 has been reported to have an endoribonuclease activity to a subset of mRNAs, such as the *c-myc* gene, through direct binding (10, 11). It remains unclear, however, precisely how these activities of G3BP1 are related to the SG-associated functions.

Ubiquitin-specific protease 10 (USP10) was originally identified as a binding partner for G3BP1 (12). It is ubiquitously expressed and is also recruited into SGs (3). USP10 is a deubiquitinase, and the substrates include tumor suppressor p53 (13). Following DNA damage, a fraction of USP10 translocates into the nucleus and then deubiquitinates and stabilizes p53. Such translocation of USP10 is regulated via phosphorylation by ataxia telangiectasia mutated (ATM) protein kinase. USP10, by deubiquitinating p53, suppresses tumor cell growth. Consistently with the activation of p53, the USP10 expression is downregulated in certain carcinomas without p53 mutations.

Using knockout and/or knockdown strategies against USP10 and G3BP1, we examined what roles G3BP1 and USP10 play in the stress response. We found that SGs inhibit apoptosis by reducing reactive oxygen species (ROS) production under stress conditions and that the formation of such functional SGs requires both G3BP1 and USP10. The overexpression and knockdown experiments indicate that USP10 possesses an antioxidant activity; however, the activity under steady-state conditions is suppressed by G3BP1, which is expressed at an excess amount relative to USP10.

Received 7 June 2012 Returned for modification 16 August 2012
Accepted 5 December 2012
Published ahead of print 10 December 2012
Address correspondence to Masahiro Fujii, fujiimas@med.niigata-u.ac.jp.
M.T. and M.H. contributed equally to this study.

doi:10.1128/MCB.00763-12

However, upon exposure to stress, SGs suppress the inhibitory activity of G3BP1 against USP10 to uncover the antioxidant activity of USP10. In addition to DNA damage, ATM is activated by its oxidation under oxidative stress and initiates antioxidant signaling by phosphorylating downstream substrates (14). The present study suggests that ATM transmits antioxidant signals partly through USP10. Collectively, the present study indicates that SGs act as components of a crucial antioxidant machinery protecting against harmful ROS-induced outcomes to mammalian cells.

MATERIALS AND METHODS

Generation of USP10 knockout mice. The details of USP10 knockout mice (RIKEN Center for Developmental Biology accession no. CDB0605K) that lack exon 3 of the *USP10* gene will be reported elsewhere.

Cell lines and culture conditions. 293T, HeLa, U2OS, Saos2, SW13, and C33A cells were cultured in Dulbecco's modified Eagle's medium (DMEM) supplemented with 10% heat-inactivated fetal bovine serum (FBS), 4 mM L-glutamine, 50 U/ml penicillin, and 50 μg/ml streptomycin (DMEM-FBS). Jurkat cells were cultured in RPMI 1640 medium supplemented with 10% heat-inactivated FBS, 4 mM L-glutamine, 50 U/ml penicillin, and 50 μg/ml streptomycin.

Establishment of immortalized MEFs. Embryonic tissues were isolated, washed with PBS, digested with 0.25% trypsin, and cultured in DMEM-FBS supplemented with 55 μM 2-mercaptoethanol. Mouse embryonic fibroblasts (MEFs) were immortalized by serial passages as described previously (15), and the cells within 40 passages were used for the experiments.

Plasmid constructs. All murine USP10 (mUSP10^{WT}), human USP10 (hUSP10^{WT}), and their mutant cDNAs were subcloned into pCMV-HA, a mammalian expression vector encoding a protein with an N-terminal hemagglutinin (HA) epitope tag (Clontech). Mutant mUSP10s (mUSP10$^{77-792}$, mUSP10$^{95-792}$, mUSP10^{F89A}, mUSP10^{C418A}, mUSP10$^{1-114}$, and mUSP10$^{1-76}$) and mutant hUSP10s (hUSP10$^{78-798}$, hUSP10$^{96-798}$, hUSP10^{F90A}, hUSP10$^{1-116}$, and hUSP10$^{1-77}$) were constructed using PCR-based mutagenesis. G3BP1^{WT} cDNA was subcloned into pFLAG-CMV-2 (Sigma-Aldrich) to construct an expression vector encoding G3BP1 with an N-terminal FLAG epitope tag. N-terminal deletion mutants of G3BP1, G3BP1$^{47-466}$, G3BP1$^{68-466}$, and G3BP1$^{105-466}$ were constructed by the PCR method and subcloned into pFLAG-CMV-2. Lentiviral expression vectors for mUSP10 and its mutants (mUSP10$^{77-792}$, mUSP10$^{95-792}$, mUSP10^{F89A}, mUSP10^{C418A}, and mUSP10$^{1-114}$) were generated by subcloning the respective cDNAs into the lentiviral vector plasmid CSII-EF-RfA with a blasticidin resistance gene (16). Lentiviral short hairpin RNA (shRNA) expression plasmids targeting human *USP10* (sh-USP10-1 and sh-USP10-3) with a puromycin resistance gene were purchased from Sigma-Aldrich.

Establishment of stable cell lines by lentiviral transduction. Vesicular stomatitis virus G (VSV-G)-pseudotyped HIV-1-based viruses were produced by the cotransfection of three plasmids (lentiviral plasmid [1.3 μg], pCAG-HIVgp [0.87 μg], and pCMV-VSV-G-RSV-Rev [0.87 μg]) into 293T cells (1.0×10^6) on a 60-mm dish by using FuGENE 6 reagent according to the manufacturer's instructions (Roche). Seventy-two hours after transfection, culture supernatants were harvested and used to infect 293T cells or MEFs in the presence of 8 μg/μl Polybrene. These cells were cultured in the selection medium containing 2 μg/ml puromycin or 5 μg/ml blasticidin, respectively, for 10 days.

RNA interference. Stealth Select RNAi small interfering RNAs (siRNAs) specific to human *G3BP1* (oligonucleotide identification no. HSS115446) and human *USP10* (oligonucleotide identification no. HSS113446) and a Stealth RNAi negative-control duplex were purchased from Invitrogen. MISSION siRNA specific to the 3′ untranslated region of human *G3BP1* (siRNA identification no. SASI_Hs01_00045804) and MISSION siRNA universal negative control were purchased from Sigma-Aldrich. Transfection was carried out with 100 to 150 pmol siRNA using Lipofectamine 2000 or Lipofectamine RNAiMAX reagents according to the manufacturer's protocol (Invitrogen).

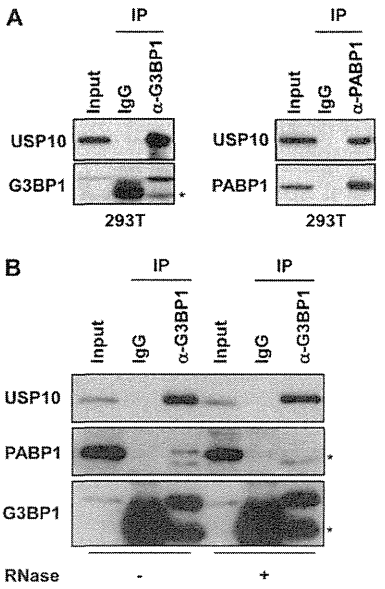

FIG 1 USP10 interacts with G3BP1 and PABP1. (A) Cell lysates prepared from 293T cells were immunoprecipitated with anti-G3BP1, anti-PABP1, and control antibodies. The cell lysate (input) and immunoprecipitates (IP) were characterized using a Western blot analysis with anti-USP10-C, anti-G3BP1, and anti-PABP1 antibodies. The asterisk indicates a nonspecific band. (B) Cell lysates prepared from 293T cells were treated with 100 μg/ml RNase at 16°C for 1 h and then immunoprecipitated with anti-G3BP1 antibody. The input and immunoprecipitates were characterized using a Western blot analysis with anti-USP10-C, anti-PABP1, and anti-G3BP1 antibodies. The asterisks indicate nonspecific bands.

Reagents and antibodies. The following reagents were purchased from the indicated companies: sodium arsenite (Wako Pure Chemical Industries), hydrogen peroxide (Sigma-Aldrich), puromycin (Calbiochem), blasticidin (Sigma-Aldrich), cycloheximide (Sigma-Aldrich), RNase (Wako Pure Chemical Industries), KU-55933 (Calbiochem), and *N*-acetylcysteine (Sigma-Aldrich). The following antibodies (at the indicated dilutions) were used in this study: anti-HA (1:2,000) (Cell Signaling Technology), anti-FLAG (1:1,000) (Sigma-Aldrich), anti-G3BP1 (1:2,000) (BD Transduction Laboratories), anti-PABP1 (1:1,000 and 1:500) (Santa Cruz Biotechnology and Abcam, respectively), anti-RACK1 (1:1,000) (Santa Cruz Biotechnology), anti-TIA-1/TIAR (1:1,000) (Santa Cruz Biotechnology), anti-ATM (1:1,000) (Calbiochem), anti-phospho-ATM (1:1,000) (Rockland Immunochemicals), and anti-α-tubulin (1:1,000) (Oncogene Research Products). The anti-USP10-C antibody (catalog no. A300-901A; Bethyl Laboratories) recognizes the central region of human USP10 and was used to detect human USP10 at a dilution of 1:2,000. The anti-USP10-N (catalog no. A300-900A; Bethyl Laboratories) and anti-USP10-163 (1:200 to 1:1,000; Cell Signaling Technology) antibodies recognize amino acids 50 to 100 and the amino acid regions surrounding Leu-163 of human USP10, respectively, and were used to detect murine USP10.

RT-PCR. Total RNA was isolated using the NucleoSpin RNA II kit (Macherey-Nagel) and reverse transcribed using the PrimeScript reverse transcription (RT) reagent kit (TaKaRa) according to the manufacturers' instructions. Then, cDNAs were amplified with 30 cycles of PCR under the following conditions: 94°C for 30 s, 55°C for 30 s, and 72°C for 20 s. The primers 5′-ACCCACAGTATATCTTTGGC-3′ and 5′-CTGTAGCT AGGAGTTGGCGG-3′ were used for PCR to detect murine *USP10* cDNA.

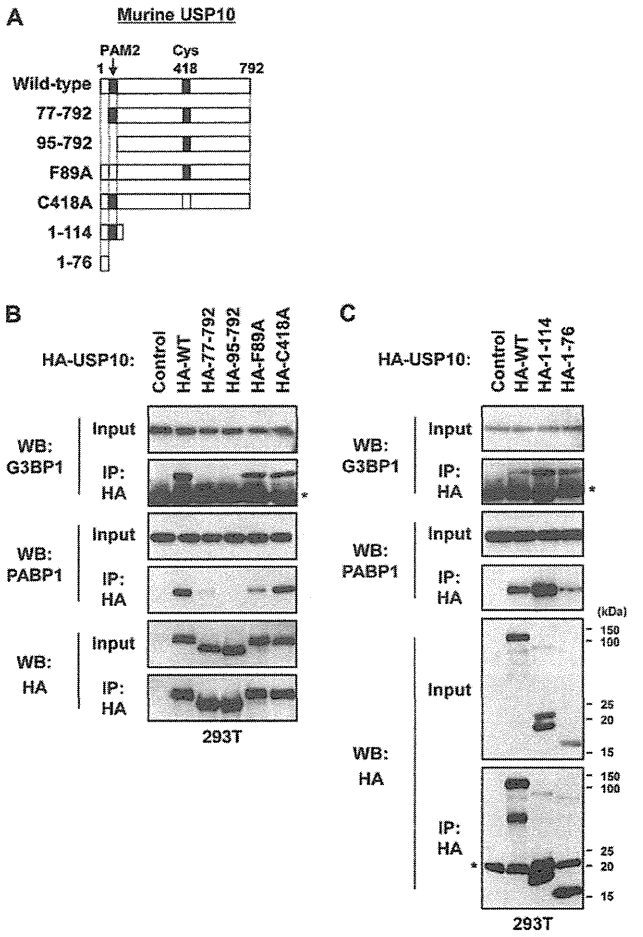

FIG 2 Domains of murine USP10 involved in binding with G3BP1 and PABP1. (A) Schematic representation of the murine USP10 (mUSP10) mutants used in this study. (B and C) 293T cells were transfected with plasmids encoding HA-tagged mUSP10 (HA-WT) and its mutants (HA-77-792, HA-95-792, HA-F89A, HA-C418A, HA-1-114, HA-1-76) as described for panel A. Cell lysates prepared from 293T cells were then immunoprecipitated with anti-HA antibody. The input and immunoprecipitates were characterized using a Western blot (WB) analysis with anti-G3BP1, anti-PABP1, and anti-HA antibodies. The asterisks indicate nonspecific bands.

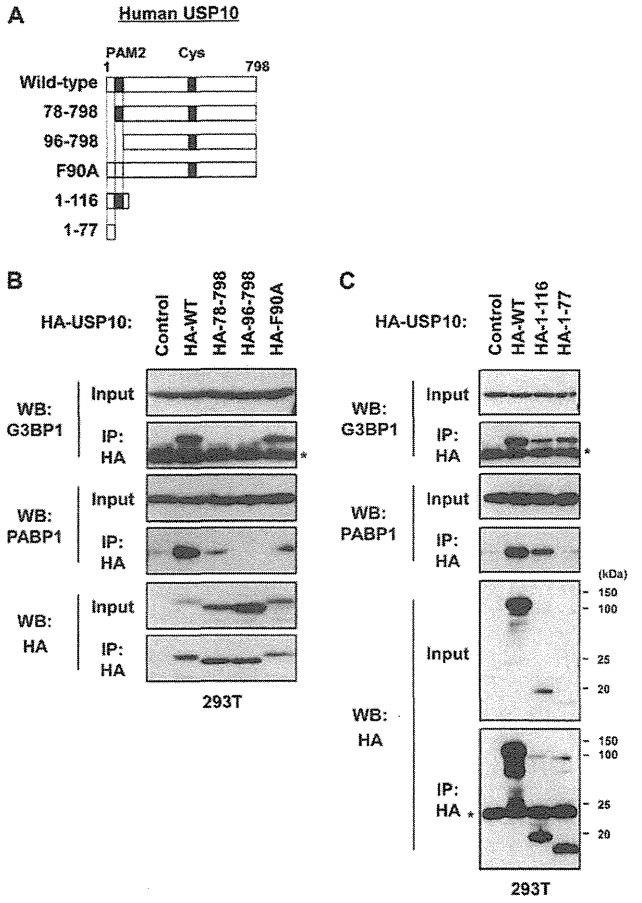

FIG 3 Human USP10 proteins interact with G3BP1 and PABP1. (A) Schematic representation of the human USP10 (hUSP10) mutants used in this study. (B and C) 293T cells were transfected with plasmids encoding HA-tagged hUSP10 (HA-WT) and its mutants (HA-78-798, HA-96-798, HA-F90A, HA-1-116, HA-1-77) as described for panel A. Cell lysates prepared from 293T cells were then immunoprecipitated with anti-HA antibody. The input and immunoprecipitates were characterized using a Western blot analysis with anti-G3BP1, anti-PABP1, and anti-HA antibodies. The asterisks indicate nonspecific bands.

Coimmunoprecipitation assay. The immunoprecipitation assay was performed as described previously (16). The cells (1.0×10^7) were lysed with ice-cold lysis buffer (1% Nonidet P-40, 25 mM Tris-HCl [pH 7.2], 150 mM NaCl, 1 mM EDTA, 1 mM phenylmethylsulfonyl fluoride, 20 μg/ml aprotinin) and incubated with the indicated antibodies. The immune complexes were precipitated by protein G-Sepharose beads (GE Healthcare). Next, the beads were washed, boiled in sodium dodecyl sulfate (SDS) lysis buffer (62.5 mM Tris-HCl [pH 6.8], 2% SDS, 1 mM phenylmethylsulfonyl fluoride, and 20 μg/ml aprotinin), and subjected to a Western blot analysis. To evaluate the RNA-dependent protein-protein interactions, the cell lysates were pretreated with 100 μg/ml RNase at 16°C for 1 h prior to incubation with the primary antibodies.

Western blot analysis. A Western blot analysis was performed as described previously (16). Briefly, the cells were lysed with SDS lysis buffer, and cell lysates (20 μg of proteins) were separated by SDS-PAGE, electrophoretically transferred onto an Immobilon polyvinylidene difluoride (PVDF) membrane (Millipore), and incubated with the indicated antibodies. Immunoreactive bands were visualized with an enhanced chemiluminescence (ECL) detection system (Amersham Pharmacia Biotech).

Immunofluorescence analysis. The cells on glass coverslips in 6-well culture plates were washed with phosphate-buffered saline (PBS), fixed with 4% formaldehyde in PBS, and permeabilized with 0.1% Triton X-100 in PBS. After being washed twice with PBS containing 3% bovine serum albumin (BSA), the cells were incubated with the first antibodies and further incubated with either Alexa Fluor 488-conjugated anti-rabbit immunoglobulin antibody (Molecular Probes) for the anti-USP10 and anti-PABP1 antibodies, Alexa Fluor 488-conjugated anti-mouse immunoglobulin antibody (Molecular Probes) for the anti-G3BP1 antibody, Alexa Fluor 594-conjugated anti-rabbit immunoglobulin antibody (Molecular Probes) for the anti-FLAG antibody, or Alexa Fluor 594-conjugated anti-mouse immunoglobulin antibody (Molecular Probes) for the anti-G3BP1, anti-PABP1, anti-RACK1, anti-HA, and anti-FLAG antibodies. Cell nuclei were stained with Hoechst 33258. The samples were then mounted in Fluoromount/Plus (Diagnostic Biosystems), and the images were analyzed with a fluorescence microscope (model BZ-8000; Keyence). More than 300 cells in three random fields were analyzed by the staining of SG markers, PABP1, and G3BP1, and the SG percentage was calculated as the ratio of SG-positive cells to the total number of cells. The intensities of anti-PABP1 staining in 60 stress granules in 6 randomly selected cells were

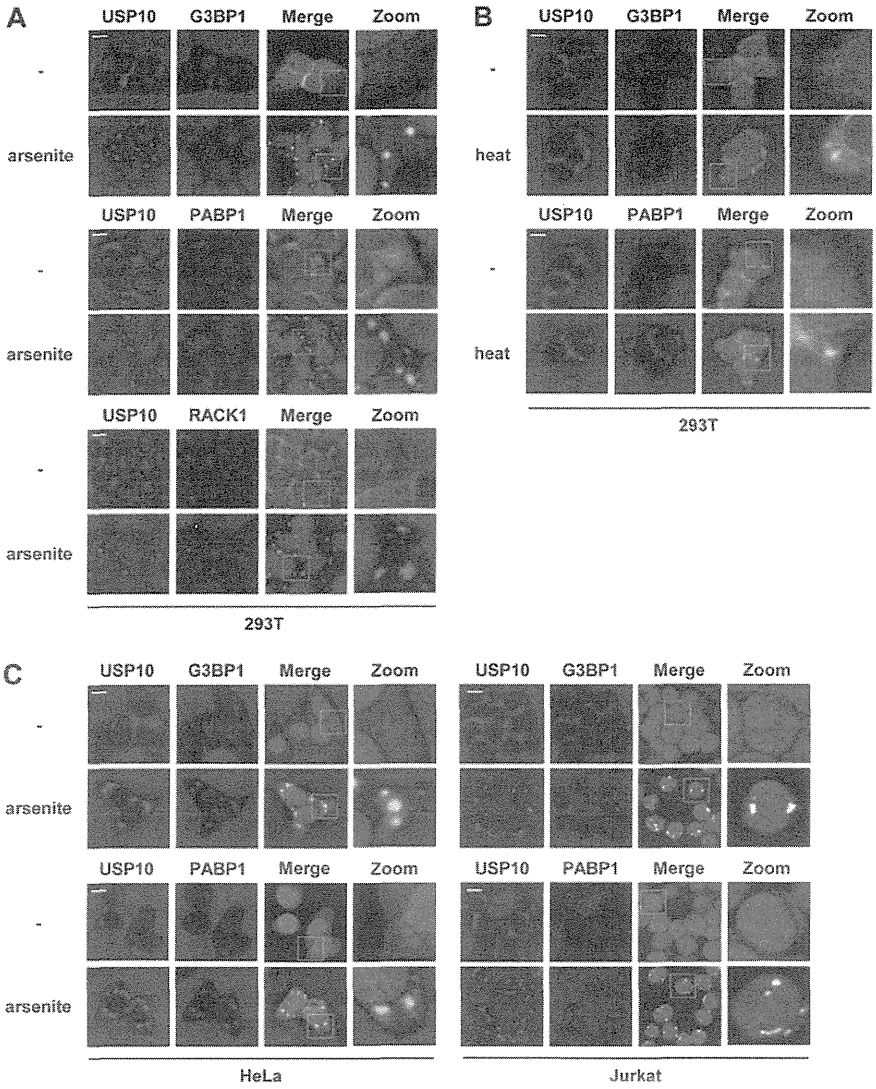

FIG 4 Subcellular th 0.5 mM sodium arsenite for 60 min or heat shock at 42°C for 60 min as indicated. The cells were then fixed and stained with anti-USP10-C (green) together with anti-G3BP1 (red), anti-PABP1 (red), or anti-RACK1 (red). Nuclei were counterstained using Hoechst 33258 (blue). The bars indicate 10 μm.

measured using a fluorescence analysis software package (BZ-II analyzer; Keyence) to determine the level of SG formation (PABP-F). Jurkat cells were washed with PBS, cultured on poly-L-lysine-coated glass slides in 6-well plates, and fixed, and the cells with SGs were visualized by a fluorescence microscope.

Quantitative determination of apoptosis. The level of apoptosis was measured by three methods. First, cells were stained with propidium iodide, and sub-G_1 DNA content was measured by flow cytometry. Second, apoptotic cells were detected with a terminal deoxynucleotidyltransferase-mediated dUTP-biotin nick end labeling (TUNEL) assay according to the manufacturer's instructions (ApoAlert DNA fragmentation assay kit; Clontech). Third, the cells cultured on coverslips in 6-well plates were fixed with 4% formaldehyde in PBS and permeabilized with 0.1% Triton X-100 in PBS. Fixed cells were stained with Hoechst 33258. After the TUNEL assay and Hoechst 33258 staining, the numbers of cells that exhibited TUNEL-positive and condensed nuclei were counted with a fluorescence microscope. More than 300 cells in three random fields were analyzed per sample.

Detection of ROS. The cells were treated with 0.5 to 1.0 mM sodium arsenite for the indicated time, washed twice with PBS, and then incubated with 5 μM 5-(and-6)-chloromethyl-2′,7′-dichlorodihydrofluorescein diacetate acetyl ester (CM-H_2DCFDA) (Molecular Probes) for 5 min at 37°C. The cells were washed twice with PBS and fixed, and CM-H_2DCFDA fluorescence in the cells was quantified using the fluorescence analysis software package (BZ-II analyzer). More than 400 cells in four random fields were analyzed, and the data are presented as the mean fluorescence intensity (DCFDA-F). ROS production in G3BP1-expressing cells was assessed by transfecting 293T cells with plasmids encoding FLAG-G3BP1^{WT} or its deletion mutants (G3BP1$^{47-466}$, G3BP1$^{68-466}$, and G3BP1$^{105-466}$). The transfected cells were incubated with 5 μM CM-H_2DCFDA for 5 min at 37°C, fixed, and incubated with anti-FLAG antibody and Hoechst 33258 stain. The fluorescence intensities of 20 cells in randomly selected fields were quantified using the fluorescence analysis software package (BZ-II analyzer).

Statistical analysis. Data were analyzed with an unpaired Student *t* test, and results are presented as means plus or minus standard deviations (SD).

RESULTS

USP10 interacts with G3BP1 and PABP1. To delineate the function of USP10, we searched for USP10-binding proteins in T cells by using a glutathione *S*-transferase fusion protein of USP10 and identified G3BP1 and PABP1 as the dominant interacting proteins (12, 17, 18; our unpublished observations). An immunoprecipitation analysis confirmed that endogenous USP10 formed a complex with G3BP1 and PABP1 in 293T cells (Fig. 1A). Pretreatment of the cell lysates with RNase prior to immunoprecipitation did not affect the interaction between G3BP1 and USP10; however, the interaction between G3BP1 and PABP1 was significantly reduced, indicating that the G3BP1 interaction with USP10 is RNA independent, whereas the interaction with PABP1 is RNA dependent (Fig. 1B). Plasmids encoding various murine USP10 (mUSP10) mutants were constructed to identify the domain of USP10 responsible for these interactions (Fig. 2A). mUSP10^{F89A} has a point mutation in the PABP-interacting motif 2 (PAM2), which is a putative binding motif for PABP1 (17). mUSP10^{C418A} has a point mutation in the cysteine protease domain, a mutation that inactivates deubiquitinating activity (12). An immunoprecipitation analysis of 293T cells showed that endogenous G3BP1 and PABP1 interacted with the amino acids 1 to 76 and 1 to 114 of mUSP10, respectively, and the PAM2 is involved in binding with PABP1 but not G3BP1 (Fig. 2B and C). The same sets of human USP10 (hUSP10) mutants showed identical binding specificities of hUSP10 to G3BP1 and PABP1 (Fig. 3).

USP10 is recruited into SGs. G3BP1 has been shown to be essential for the assembly of SGs under various stress conditions (5, 7, 8). Therefore, we next examined whether USP10 is localized in SGs. USP10 was found to be diffusely localized in the cytoplasm of 293T cells, and the distribution was almost identical to that of G3BP1. Upon treatment with 0.5 mM arsenite, USP10 was detected predominantly in the SGs containing G3BP1 in 293T cells (Fig. 4A). The granules also recruited PABP1 and RACK1, which are other SG marker proteins (Fig. 4A). Similar recruitment of USP10 into SGs was also detected in 293T cells exposed to heat shock (Fig. 4B) and in HeLa and Jurkat cells treated with arsenite (Fig. 4C). These results show that USP10 is recruited into SGs in cells exposed to stress. This recruitment of USP10 into SGs is consistent with the findings of a previous study (3).

USP10 inhibits arsenite-induced apoptosis. To investigate whether USP10 is involved in SG-associated functions, USP10 knockout mice were generated, and USP10-deficient mouse embryonic fibroblasts (*USP10*$^{\Delta/\Delta}$ MEFs) were established (Fig. 5). The *USP10*$^{\Delta/\Delta}$ mice had the deletion of the *USP10* exon 3 and were expected to encode the 30 N-terminal amino acids of USP10 and an additional 11 amino acids derived from the out-of-frame sequence of exon 4 (Fig. 5A). An RT-PCR analysis detected the expected size of the fragments corresponding to the *USP10* mutant mRNA with a deletion of exon 3 in the *USP10*$^{\Delta/\Delta}$ MEFs (Fig. 5A and B). A Western blot analysis showed that two USP10 antibodies that recognize distinct N-terminal regions of USP10 (located downstream of the *USP10* exon 3) detected USP10 proteins in the *USP10*$^{+/+}$ MEFs but not in the *USP10*$^{\Delta/\Delta}$ MEFs (Fig. 5C). Treatment with arsenite (1 mM) induced SGs in *USP10*$^{\Delta/\Delta}$ MEFs, but there were fewer SGs, and they were smaller than those in *USP10*$^{+/+}$ MEFs (Fig. 6A to C). In addition, the SGs in the *USP10*$^{\Delta/\Delta}$ MEFs disappeared much more rapidly than those in the *USP10*$^{+/+}$ MEFs (Fig. 6B). USP10 deficiency in MEFs, however, had little effect on the levels of G3BP1 and PABP1 (Fig. 5C). Low SG-forming activity was recapitulated in USP10 knockdown 293T cells established by shRNA under stress conditions (arsenite, heat shock) (Fig. 6D to F). These results indicate that USP10 is not essential for the formation of SGs in MEFs, but they demonstrate that it does promote their formation.

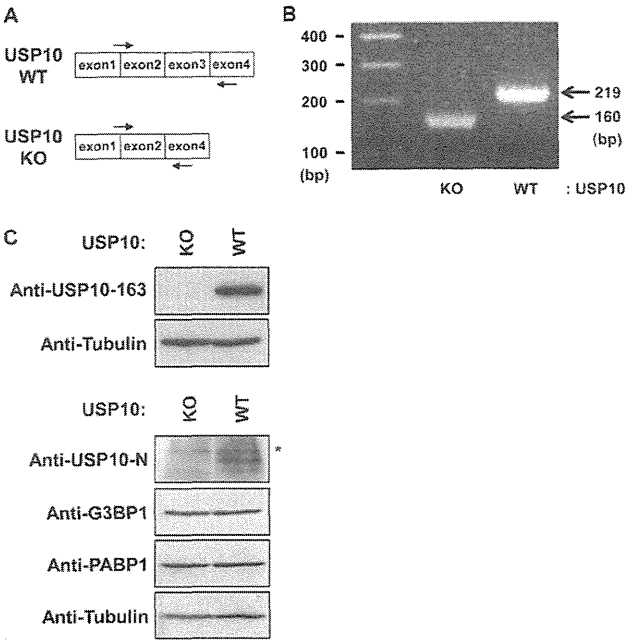

FIG 5 Characterization of the *USP10* null allele. (A) The boxes indicate exons 1 to 4 of the murine *USP10* genome. The arrows indicate the positions of the primer sets in the *USP10* genome. (B) An RT-PCR analysis of murine *USP10* mRNA in the *USP10*$^{\Delta/\Delta}$ (knockout [KO]) and *USP10*$^{+/+}$ (wild-type [WT]) MEFs. The arrows and numbers indicate the PCR products and expected sizes, respectively. (C) Cell lysates prepared from *USP10*$^{\Delta/\Delta}$ (KO) and *USP10*$^{+/+}$ (WT) MEFs were characterized using a Western blot analysis with anti-USP10, anti-G3BP1, anti-PABP1, and anti-α-tubulin antibodies. Anti-USP10-163 and anti-USP10-N antibodies (upper blots, Cell Signaling Technology; lower blots, Bethyl Laboratories) recognize the amino acid regions surrounding Leu-163 and amino acids 50 to 100 of human USP10, which are located downstream of *USP10* exon 3. The asterisk indicates a nonspecific band.

SGs play an essential role in the recovery of cells from some types of stress, and the inability to form SGs induces apoptosis (1, 7). Therefore, the apoptosis sensitivity of *USP10*$^{\Delta/\Delta}$ MEFs was examined. Arsenite induced apoptosis in *USP10*$^{\Delta/\Delta}$ MEFs, and the level was much higher than that of *USP10*$^{+/+}$ MEFs (Fig. 7). The apoptosis induced in *USP10*$^{\Delta/\Delta}$ MEFs was totally inhibited by *N*-acetylcysteine (NAC), a precursor of the ROS scavenger glutathione, indicating that USP10 inhibits ROS-dependent apoptosis in MEFs (Fig. 8A). Therefore, the kinetics of ROS production in *USP10*$^{\Delta/\Delta}$ MEFs treated with arsenite were monitored. The amounts of ROS in *USP10*$^{\Delta/\Delta}$ and *USP10*$^{+/+}$ MEFs were equivalently reduced 30 min after arsenite exposure, but the amount of ROS in *USP10*$^{\Delta/\Delta}$ MEFs at 60 min was elevated more than that in *USP10*$^{+/+}$ MEFs (Fig. 8B and C). These results indicate that arsenite reduces ROS production for 60 min in MEFs, and the ROS reduction within 30 min is independent of USP10, but the ROS reduction from 30 to 60 min and thereafter is dependent on USP10 (Fig. 8B and C). Collectively, these results indicate that USP10 plays important roles in arsenite-induced SG formation,

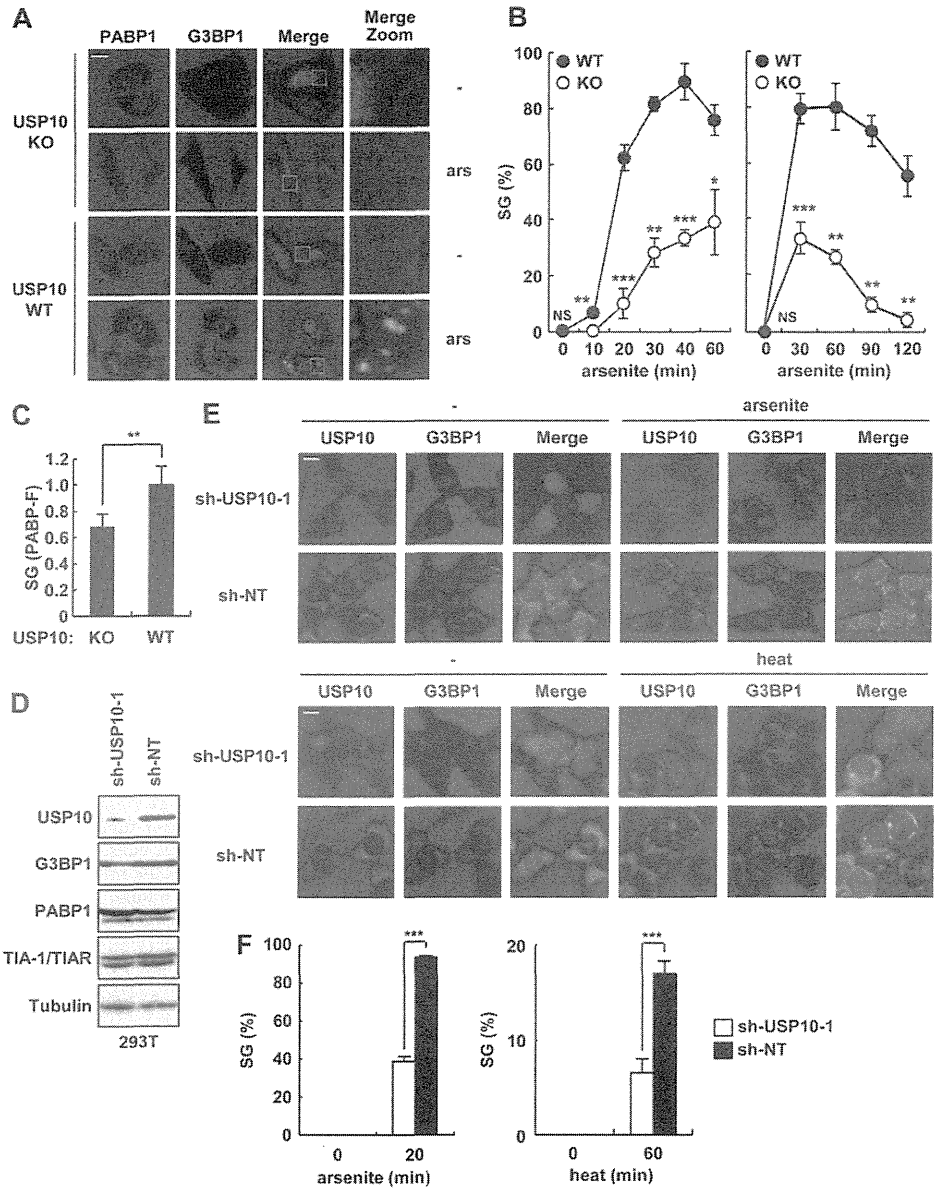

FIG 6 USP10 plays critical roles in SG formation. (A and B) *USP10*$^{\Delta/\Delta}$ (KO) and *USP10*$^{+/+}$ (WT) MEFs were treated with 1 mM sodium arsenite for 60 min (A) or the indicated times (B). The cells were fixed and then stained with anti-PABP1 (green) and anti-G3BP1 (red) antibodies and Hoechst 33258 (blue). Staining was visualized with a fluorescence microscope (A). The bar indicates 20 μm. (B) The proportions (percentages) of cells containing SGs at the indicated time points. (C) Cells were treated with 1 mM sodium arsenite for 40 min, and the levels of PABP1 fluorescence in 60 SGs (PABP-F) were quantitatively determined by the fluorescence analysis software. (D) 293T cells were infected with lentiviruses encoding human *USP10* shRNA (sh-USP10-1) or control nontargeting shRNA (sh-NT), and the cells were cultured in the presence of puromycin. Cell lysates were prepared from selected cultures and characterized using a Western blot analysis with anti-USP10-C, anti-G3BP1, anti-PABP1, anti-TIA-1/TIAR, and anti-α-tubulin antibodies. (E) USP10 knockdown and control cells were either treated with 0.5 mM sodium arsenite for 20 min (upper panels) or exposed to heat shock at 42°C for 60 min (lower panels). The cells were then stained with anti-USP10-C (green) and anti-G3BP1 (red) antibodies and Hoechst 33258 (blue). The bars indicate 10 μm. (F) SG percentages. In all panels, the values denote the means ± SD. *, $P < 0.05$; **, $P < 0.01$; ***, $P < 0.001$; NS, not significant.

suppression of ROS elevation, and ROS-dependent apoptosis in MEFs.

SGs reduce ROS production. Hydrogen peroxide (H_2O_2) is an oxidative stress (19) that does not induce SGs in MEFs (Fig. 9A). This study next examined the function of USP10 to a stress without inducing SGs. H_2O_2 also induced apoptosis in *USP10*$^{\Delta/\Delta}$ MEFs, but unlike the results with arsenite, the level was equivalent to that in *USP10*$^{+/+}$ MEFs (Fig. 9B). These results suggest that USP10 inhibits arsenite-induced apoptosis as a result of the formation of SGs. *USP10*$^{\Delta/\Delta}$ MEFs stably expressing mUSP10s were established to test this hypothesis (Fig. 10A). The expression of mUSP10^{WT} in *USP10*$^{\Delta/\Delta}$ MEFs increased SG formation and inhibited ROS production and apoptosis (Fig. 10B to D), confirming that USP10 plays a role in all three activities. mUSP10^{F89A} and